AMERICAN JOURNAL OF PHARMTECH RESEARCH
Journal home page: http://www.ajptr.com/

Microwave-Assisted Green Synthesis and Anticancer Activity of Gold and Silver Nanoparticles Using Root Extract of *Hymenodictyon Orixense* (Roxb.)

Riya Sahu*, Vinod D. Rangari
Department of Pharmacy, Guru Ghasidas Vishwavidyalaya, India.

ABSTRACT

This study reports the eco-friendly synthesis of gold (AuNPs) and silver (AgNPs) nanoparticles using the alcoholic root extract of *Hymenodictyon orixense*. The use of *H. orixense* root extract offers a novel approach in green synthesis, as it has been relatively underexplored.The nanoparticles were synthesized via a microwave-assisted method, utilizing extract of *H. orixense* as a reducing and stabilizing agent. The phytochemicals present in the extract played a crucial role in reducing the metal ions and stabilizing the resulting nanoparticles. The synthesis was confirmed by a visual colour change and characterized using various physicochemical techniques. The synthesized gold and silver nanoparticles showed characteristic surface plasmon resonance peak at 544 nm and 427 nm, respectively. They exhibited significant cytotoxicity against MCF-7 (breast cancer), A549 (lung cancer), and HepG2 (liver cancer) cell lines, with AuNPs exhibiting slightly higher cytotoxicity compared to AgNPs. Statistical analysis using ANOVA revealed that the cytotoxic effects of both AuNPs and AgNPs were significant ($p < 0.001$) compared to the untreated control cells. The study demonstrates the potential of *H. orixense*-mediated green synthesis in producing nanoparticles with promising anticancer properties. Quantitative comparisons revealed that AuNPs had lower IC50 values and higher antioxidant activity than extract and AgNPs. The significant cytotoxicity exhibited by these nanoparticles suggests their potential for further development as therapeutic agents. However, further studies are needed to elucidate the underlying mechanisms, optimize the synthesis process, and evaluate the *in vivo* efficacy and safety of these nanoparticles.

Keywords: *Hymenodictyon orixense*, root extract, gold nanoparticle, silver nanoparticle, microwave-assisted green synthesis, anticancer activity.

*Corresponding Author Email: riyasahu2609@gmail.com
Received 13 January 2026, Accepted 26 January 2026

Please cite this article as: Sahu R *et al*., Microwave-Assisted Green Synthesis and Anticancer Activity of Gold and Silver Nanoparticles Using Root Extract of Hymenodictyon Orixense (Roxb.). American Journal of PharmTech Research 2026.

INTRODUCTION

Nanotechnology is a scientific field that focuses on understanding and manipulating matter at the nanoscale (1-100 nm) to develop novel materials, devices, and processes [1,2]. Nanomedicine, a subset of nanotechnology, applies these principles to biological systems for diagnosis, medical treatment, monitoring, and regulation [3,4].

The production, characterization, and applications of various types of nanoparticles (NPs) are the primary focus of nanotechnology [5]. Figure 1 represents a diagrammatic representation of the nanoparticles. NPs are frequently made from noble metals, such as gold, silver, or platinum, using a range of physical and chemical methods [6] as represented in Figure 2. However, these methods are not environmentally benign. Green synthesis, using biological systems like plants, algae, bacteria, and fungi, offers a promising alternative [7]. Plant-based nanoparticle green synthesis is particularly attractive due to its simplicity, safety, and scalability [8].

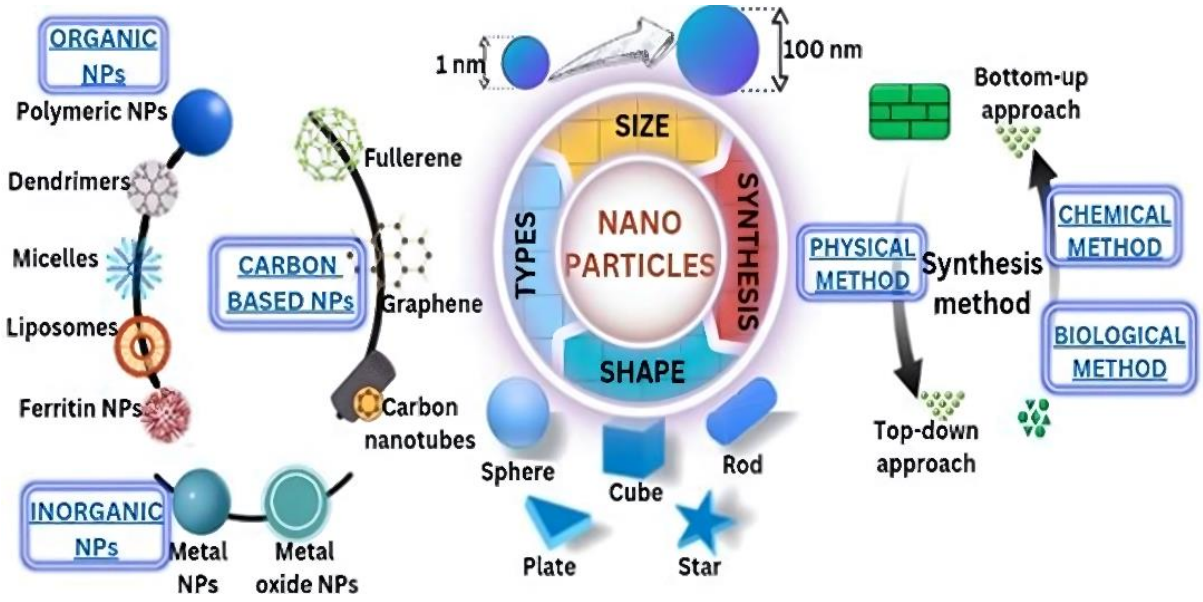

Figure 1: Diagrammatic representation about Nanoparticles.

The principles of green chemistry and sustainable development emphasize the use of environmentally friendly solvents, reducing agents, and stabilizing agents to minimize the environmental impact of chemical processes [9,10]. The green synthesis of AuNPs and AgNPs aligns with these principles, offering a promising approach for developing eco-friendly and biocompatible nanoparticles for biomedical applications [11].

Plant extracts can be used to synthesize AuNPs and AgNPs, offering a simple and eco-friendly approach. Biomolecules in plant extracts, such as phenols and flavonoids, can act as reducing agents, allowing for the synthesis of nanoparticles with specific sizes, shapes, and compositions [12,13]. It is acknowledged that NPs derived from plants have higher biological potential and can

be utilized in various fields, including agriculture, food science and technology, bioengineering, cosmetics, and nanomedicine, as well as human health protection [14,15]. They are also thought to be less likely to have negative side effects in humans than NPs synthesized chemically [16].

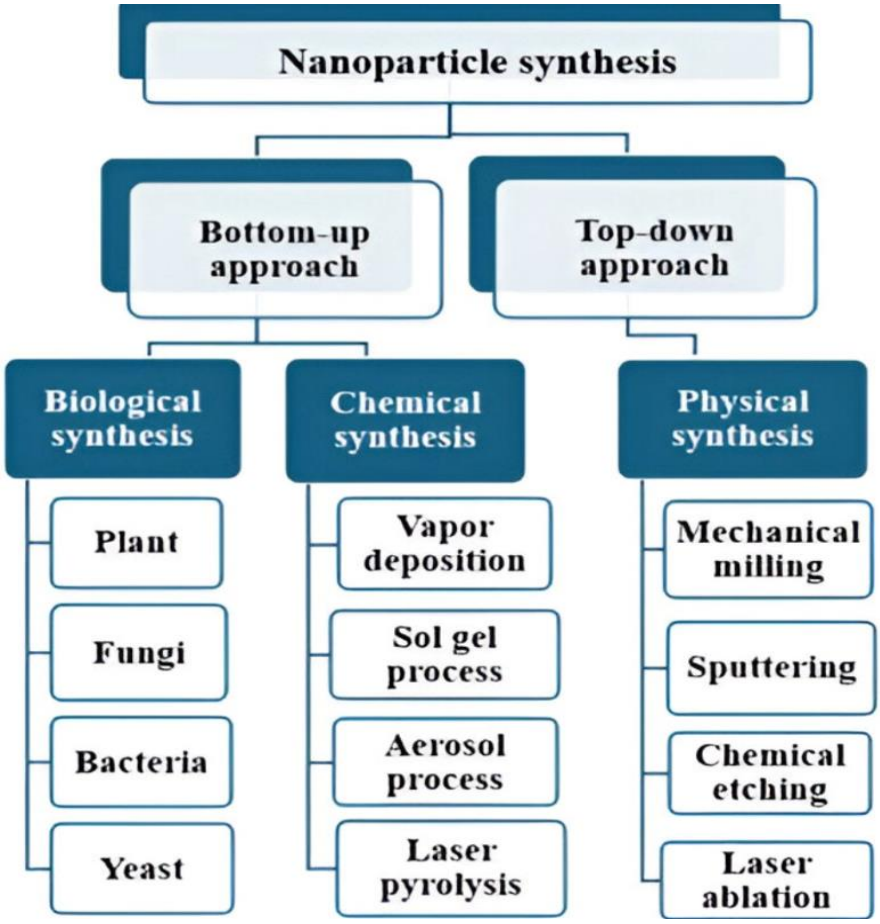

Figure 2: Diagrammatic representation of method of nanoparticle synthesis.

To ensure reproducibility in their manufacture, biological activity, and safety, these NPs must be accurately and completely characterized [17]. Various physicochemical techniques are employed for this purpose, including Ultraviolet-visible spectroscopy (UV-Vis.), Fourier transform infrared spectroscopy (FTIR), Dynamic light scattering (DLS), Transmission electron microscopy (TEM), Scanning electron microscopy (SEM), Atomic force microscopy (AFM), X-ray diffractometer (XRD), Energy dispersion analysis of X-ray (EDAX), Thermal gravimetric differential thermal analysis (TG-DTA), or Nuclear magnetic resonance (NMR). These techniques enable precise characterization of the synthesized nanoparticles, ensuring their quality and safety for various applications [18].

Gold and silver have been used as alternatives to pharmacological substances for centuries. The unique properties of noble metal nanoparticles, particularly gold and silver, make them attractive for various biomedical applications. Their small size enables simultaneous diagnostics and

therapies, and their high catalytic efficiency and exceptional biocompatibility offer advantages over synthetic medications [19].

Gold nanoparticles (AuNPs) have gained significant attention in scientific studies due to their chemical stability, lack of cytotoxicity, and highly tunable chemical and physical properties [20]. AuNPs can be synthesized into various geometries, including hexagonal platelets, nanorods, nanotriangles, and nanoprisms. Their ability to enter tissues readily due to their nanosize makes them effective medication carriers, and their capacity to bind with biomarkers has led to their use in targeted drug delivery applications. AuNPs have also been used to image tumor tissues in vivo and as sensing probes in analytical applications [21]. The synthesis of gold nanoparticles involves the reduction of gold metal ions by reducing agents, which can be chemical moieties in biogenic complexes. Biomolecules such as proteins, phenols, and flavonoids play a crucial role in the reduction of metal ions and the stabilization of gold nanoparticles in plant extracts [22]. This green synthesis approach offers a promising method for producing AuNPs with specific properties and applications [23].

Silver nanoparticles (AgNPs) have gained significant attention due to their flexibility and versality in various applications [24]. With over 313 consumer products containing nano silver released onto the market, AgNPs can be integrated into various mediums and applied in liquid, colloidal, and solid forms. The size and shape of AgNPs determine their optical properties, resulting in different colours. AgNPs exhibit superior physical characteristics, including high thermal conductivity, chemical stability, nonlinear optical behaviour, and strong catalytic activity [25]. The vast surface area of AgNPs enables functionalization with various ligands, making them suitable for diverse applications [26]. However, the widespread use of AgNPs in many fields necessitates a thorough understanding of their toxicity to assess the risks associated with their use. Plant-derived AgNPs are among the simplest to produce, requiring a silver metal ion solution and a reducing biological agent. Biomolecules such as polysaccharides, vitamins, amino acids, proteins, phenolics, saponins, alkaloids, and/or terpenes can be used to reduce and stabilize Ag ions, offering a cost-effective and environmentally friendly approach. Nearly every plant has the potential to be used in the preparation of AgNPs, making this method a promising avenue for future research and development [27].

Hymenodictyon orixense (Roxb.), also known as “Bhorsal,” is a member of the Rubiaceae family, renowned for its wound-healing properties [28]. Additionally, it exhibits antimicrobial, anticoagulant, anti-inflammatory, and sunblock properties [29]. This plant is widely distributed in deciduous forests, plains, and rain forests in various regions, including India, Thailand, and Indo-

Malaysian Western Ghats. In India, abundantly found in Maharashtra, Kerala, Tamil Nadu, Assam, Meghalaya, Odisha, and Chhattisgarh. Figure 3 (a-f) represents the different parts of *H. orixense*. The stem bark of *H. orixense* contains tannin, hymenodictine (a toxic alkaloid), aesculin (a bitter substance), an apioglucoside of scopoletin, and hymexelsin as represented in Figure 4. The roots have been found to contain anthraquinones, rubiadin and its methyl ether, lucidin, damnacanthal, nordamnacanthal, 2 benzyl zanthopurpurin, anthragallol, soranjidol, and morindone [30,31] as represented in Figure 5. These phytochemicals may play a crucial role in the plant's medicinal properties and potentially act as reducing and stabilizing agents in nanoparticle synthesis.

Figure 3: Different plant parts of *Hymenodictyon orixense*: (a) Inflorescence, (b) Branches, (c) Leaves, (d) bark, (e) Stipule, (f) Shoot apex.

Around the world, traditional medical systems have utilized *H. orixense* bark and leaves primarily to treat various ailments, including smallpox, fever, sores, atrophy, and lactation complaints. They have also been used to treat burning sensations in the chest, carbuncle and emaciation, and used as a decoction for diarrhoea. Leaves are used to treat inflammatory diseases, ulcers, tonsillitis, sore throats, and sialitis. The plant's inner bark has been used as an astringent, febrifuge, and antiperiodic, particularly for tertian ague. It is additionally utilized to treat night blindness and as a quinine alternative. Hemorrhoids (piles) are treated orally with the crushed and powdered bark [30].

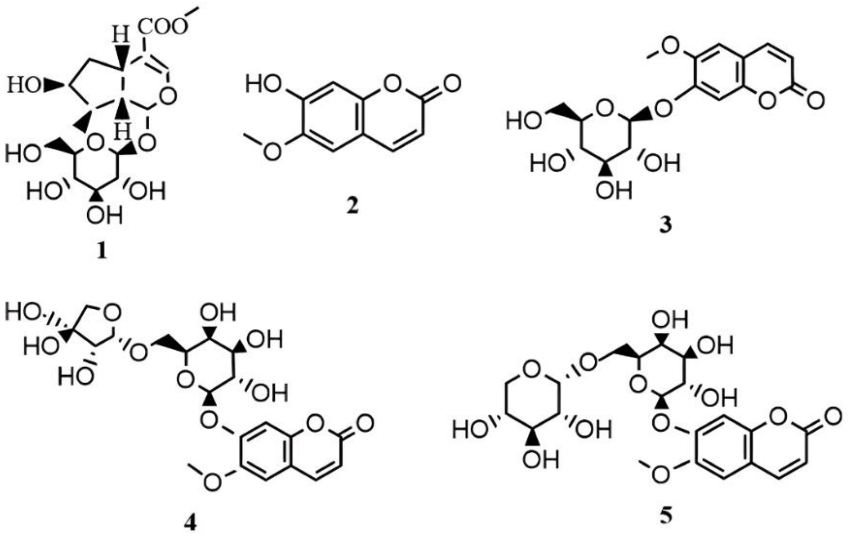

Figure 4: 1. Loganin, 2. Scopoletin, 3. Scopolin, 4. Hymexelsin, 5. Scopoletin7-O- β-D-xylopyranosyl-(1 1→6)-β-Dglucopyranoside.

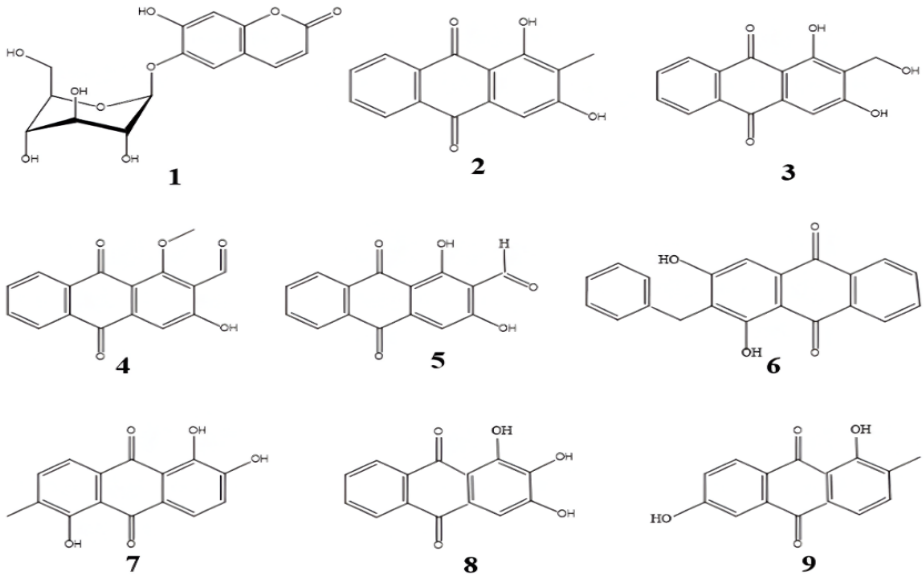

Figure 5: 1. Aesculin, 2. Rubiadin, 3. Lucidin, 4. Damnacanthal, 5. Nordamnacanthal, 6. 2-benzylzanthopurpurin, 7. Morindone, 8. Anthragallol, 9. Soranjidol.

Following the completion of a thorough literature review, it was found that root of *H. orixense* had never before been used to prepare AuNPs and AgNPs. This study aimed to bridge this gap by exploring the green synthesis, characterization, and biological activity of *H. orixense*-derived AuNPs and AgNPs. It is important to note that this plant's chemical compounds may function as capping, reducing, and stabilizing agents when nanoparticles are formed, hence boosting biological activity. Using microwave-assisted green synthesis, *H. orixense* root extract is used in the current study to produce nanoparticles as a capping, reducing, and stabilizing agents. UV-Visible spectroscopy, particle size, zeta potential, FTIR, XRD, SEM, and TGA were used to characterize the produced nanoparticles. Furthermore, *invitro* anticancer activity on breast cancer MCF-7, lung cancer A549, and liver cancer HepG2 cell lines using MTT assay were studied. Multiple biological activity in *H. orixense* have also been documented by researchers, including apoptosis, cytotoxic activities [32], antiproliferative activity [33,34], anti-prostate cancer effect and antagonistic effects [35], Anti-malarial activity [36], antifungal, antibacterial activities, membrane stabilizing, analgesic, antipyretic, moderate amylase inhibition activities and central nervous system (CNS) depressing activity on Swiss mice [37], anti-inflammatory effects [38], effective larvicidal activity [39], Acetylcholinesterase inhibitory activity [40], antioxidant and anti-HIV properties [41,42], antimicrobial activities [43], and also used for the treatment of Cervix Carcinoma [44]. These findings drove us to investigate the several biological activities of *H. orixense*-mediated AuNPs and AgNPs.

MATERIALS AND METHOD

Chemicals and reagents

Gold (III) chloride trihydrate, silver nitrate, Folin-ciocalteu reagent, and DPPH (2,2-diphenyl-1-picryl-hydrazylhydrate) was purchased from Central Drug House Pvt Ltd. India (CDH). Ascorbic acid, Gallic acid, Quercetin, Tannic acid, Ethanol, Methanol, Sodium carbonate, Sodium nitrate, Aluminum chloride, Mercuric chloride, Potassium iodide, Iodine, Lead acetate, NaOH, Ferric chloride, α-naphthol, H_2SO_4, Chloroform, Acetonitrile, Acetone, Ninhydrin, Potassium dichromate, Silica gel G, Toluene, Ethyl acetate, and Formic acid was purchased from HIMEDIA Co. Ltd. India.

Collection, drying, and processing of plant material

The root bark of *H. orixense* was collected from the Achanakmar Amarkantak Biosphere Reserve, Chhattisgarh, India. For identification purposes, the *H. orixense* flowering branch was collected for the herbarium and identified by the Plant Identification Cell, Department of Botany

(Bot/GGV/2022/39A), Guru Ghasidas Vishwavidyalaya, Koni Bilaspur, Chhattisgarh, India**.** The collected root bark was cleaned, washed, and air-dried at room temperature [45].

Preparation of plant extract

The dried samples were then powdered, and the coarse powder was subjected to Soxhlet extraction as represented in Figure 6. Thirty grams of the powdered root bark were extracted, using 500mL of ethanol as a solvent, with a temperature range of 60-70°C for 48 hours, until it was colourless, and the resulting extract was collected and dried [46]. The dried extract, known as *H. orixense* root bark ethanolic extract (HOEE), was stored in a refrigerator for further use.

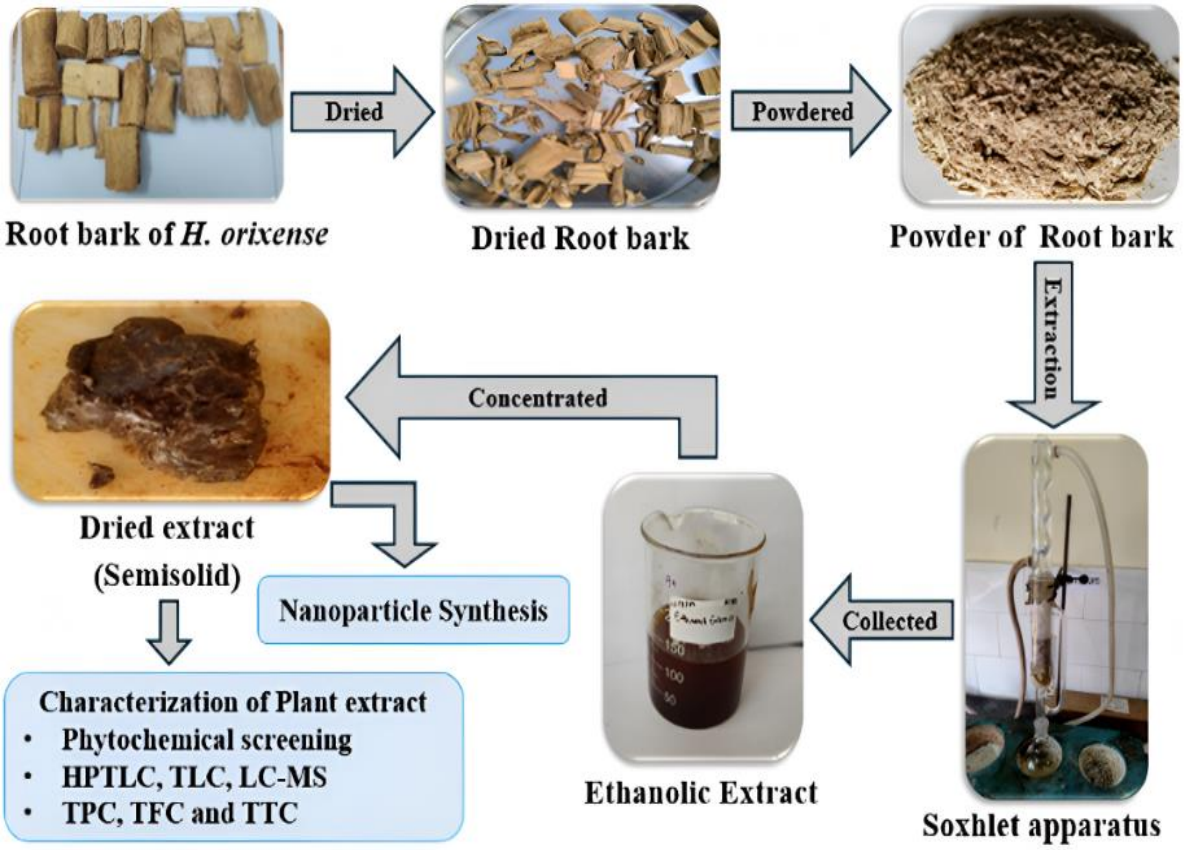

Figure 6: Collection and extraction of *H. orixense* root bark.

Preliminary phytochemical screening

The HOEE was subjected to preliminary phytochemical screening to determine the presence of various bioactive compounds, including alkaloids, saponins, flavonoids, tannins, quinones, carbohydrates, phytosterols, phenolic compounds, and coumarins. Standard chemical tests were followed to detect these compounds [47].

HPTLC analysis

The *H. orixense* ethanolic extract was sent to Anchrom Enterprises Pvt. Ltd. Mumbai, India for High-Performance Thin Layer Chromatography (HPTLC) fingerprint analysis**.** For sample

preparation, 30 mg of the extract was mixed with 3 mL of ethanol: water (10mg/ml) and sonicated for 10 minutes, then centrifuged at 2000 rpm for 5 minutes. The supernatant was applied to a TLC plate, and a developing chamber (TTC 20 x 10cm) was used with a mobile phase consisting of n-butanol: methanol: water in the ratio of 3:1:1 v/v/v. The chamber was saturated for 20 minutes before development. The plate was dried and visualized using a CAMAG TLC VISUALIZER under three conditions: R White (Image at White Light), R 254 (Image at 254 nm wavelength), and R 366 (Image at 366 nm wavelength) [48]. The plate was then derivatized with Anisaldehyde Sulphuric Acid (ASR) reagent and analyzed using a CAMAG TLC DERIVITIZER. The Rf values of the spots were calculated using WinCATS HPTLC software. Spectral data were collected using a TLC Scanner and documented. This HPTLC analysis aimed to generate a fingerprint profile of the *H. orixense* ethanolic extract, which can help identify and characterize the bioactive compounds present in the extract [49].

Thin layer chromatography (TLC)

A slurry of silica gel was prepared by adding water to it, then poured onto the center of a plate and spread evenly to create a TLC plate of uniform thickness. The manually prepared plates were activated by heating them to 110-120℃ in an oven for 30 minutes before sample application [50]. Chloroform: Acetonitrile (2:1 v/v) was selected as the mobile phase based on literature surveys [51]. The prepared solvent system was placed in a chamber for saturation for 15-20 minutes prior to chromatography. The sample was prepared by dissolving the extract in a suitable solvent, then applied to the TLC plate using a capillary tube, 1.5 cm from the bottom edge. The plate was placed in a saturated chamber, and the solvent front was allowed to reach up to 6 cm of the plate length. Detection of spots and scanning were done using UV chambers, iodine chambers, and various spraying reagents. The R_f value was calculated and compared with references [52].

Liquid chromatography-Mass spectroscopy (LC-MS)

The LC-MS analysis was performed using an Agilent 1290 II HPLC and 6470 triple quadrupoles (Agilent technologies, Santa Clara, CA, USA) equipped with a quaternary pump (DEBA301418(G7104A), column compartment (DEAED28863 (G7116A), and vial autosampler (DEBA905681(G7129B)). Data acquisition was performed using MassHunter software (V10.1). Chromatographic separation was carried out on an Agilent ZORBAX Eclipse Plus C8 column (100 × 4.6 mm, 5 µm) using a gradient elution program with a mobile phase containing water (0.1% acetic acid) (A) and methanol (B) as follows: % B (time): 5% (0min), 5% (0.2min), 95% (5min), 95% (8min), 5%(10min), and 5%(5min). The flow rate, column temperature, and injection volume were 0.4mL/min, 45 ºC, and 10µL, respectively. Agilent Jet Stream electrospray ionization (ESI)

and an atmospheric pressure chemical ionization source (APCI) were used for the analysis of the HOEE (*H. orixense* root bark ethanolic extract) compound [53].

Quantitative analysis

Total phenolic content (TPC)

The total phenolic content (TPC) in the extract was determined using the Folin-Ciocalteu method. A volume of 1 mL of the sample extract (1 mg/mL in methanol) was combined with 5 mL of 10% Folin-Ciocalteu reagent and kept aside for 5 minutes. Then, 4 mL of Na_2CO_3 (7.5% w/v) was added, and the mixture was vortexed and kept in the dark condition for 60 minutes at room temperature. The absorbance was measured at 765 nm against a blank (solution with methanol instead of extract) using a UV-1800 Shimadzu UV- Spectrophotometer. A standard solution of gallic acid (10, 20, 30, 40, and 50 µg/mL in methanol) was prepared in the same manner, replacing the extract with gallic acid solution, to draw the standard curve. The experiment was carried out in duplicate, and the TPC was calculated from the gallic acid standard curve ($y = 0.0088x + 0.0072$, $R^2 = 0.9877$) and expressed as mg of gallic acid equivalent per gram of dried extract [54].

Total flavonoid content (TFC)

The total flavonoid content (TFC) of the extract was determined using an aluminium chloride colorimetric assay. 1 mL aliquots of sample solution (1 mg/mL in methanol) were mixed with 4 mL distilled water, followed by the addition of 300 µL of sodium nitrate solution (5% w/v). The mixture was vortexed and incubated for 5 minutes, then 300 µL of aluminium chloride (10% w/v) solution was added. The solution was vortexed and incubated for 6 minutes, followed by the addition of 2 mL of sodium hydroxide (1M). The volume was made up to10 ml with distilled water, and the solution was vortexed and incubated for 15 minutes. The absorbance was measured at 510 nm against a blank (solution with methanol instead of extract) using a UV-1800 Shimadzu UV-Spectrophotometer. A calibration curve was constructed using different concentrations of quercetin (10, 20, 30, 40, and 50 ug/mL in methanol). The experiment was carried out in duplicate, and the TFC was calculated from the quercetin standard curve ($y = 0.0006x + 0.001$, $R^2 = 0.9735$) and expressed as mg of quercetin equivalent (QE) per gram of dried extract [55].

Total tannin content (TTC)

The total tannin content (TTC) in the extract was determined using the Folin-Ciocalteu method. 1 mL of extract (1 mg/mL) was mixed with 500 µL of Folin-Ciocalteu reagent (10% v/v), 1 mL of sodium carbonate (35% w/v), and 7.5 mL of distilled water. The mixture was vortexed and incubated for 30 minutes at room temperature, then the absorbance was measured at 700 nm using a UV-1800 Shimadzu UV-Vis Spectrophotometer against a blank (distilled water instead of

extract). The TTC was expressed as mg of tannic acid equivalent (TAE) per gram of dried extract, calculated from the standard curve using different concentrations of tannic acid (10. 20, 30, 40, and 50 µg/mL). The experiment was carried out in duplicate, and the TTC was calculated from the tannic acid standard curve ($y = 0.0046x - 0.0077$, $R^2 = 0.9975$) [56].

Synthesis of gold and silver nanoparticles

H. orixense-mediated gold and silver nanoparticles were biosynthesized using the microwave irradiation method. The microwave-assisted green synthesis offers several advantages over previously reported methods, including reduced reaction time, eco-friendliness, and potential for large-scale production [57–59]. The unique phytochemical profile of the extract contributes to the stabilization and bioactivity of the nanoparticles.

Initially, various trial syntheses were carried out in a microwave (Catalyst^{TM} CATA R) by mixing an alcoholic root extract of *H. orixense* with an aqueous solution of 1mM Gold (III) chloride trihydrate for the synthesis of gold nanoparticles, until the colour changed from blackish-brown to purple after irradiation. The produced AuNPs were then confirmed using a UV-1800 Shimadzu UV-Spectrophotometer. The optimum conditions for the synthesis of *H. orixense*-mediated gold nanoparticles (HOAuNPs) were found to be: microwave power 480-watts, extract: metal salt solution (1 mM) in the ratio 1:9 (v/v), and irradiation time 90 seconds, due to the small size and stability of the AuNPs.

Similarly, silver nanoparticles were synthesized by mixing an alcoholic root extract of *H. orixense* with an aqueous solution of 1mM Silver Nitrate, until the colour changed from pale yellow to dark brown after irradiation. The produced AgNPs were then confirmed using a UV-1800 Shimadzu UV-Spectrophotometer. The optimum conditions for the synthesis of *H. orixense*-mediated silver nanoparticles (HOAgNPs) were: microwave power 800-watts, extract: metal salt solution (1 mM) in the ratio 1:9 (v/v), pH of the solution 8 (0.01 M NaOH), and irradiation time 5 minutes, due to the small size and the stability of the AgNPs [19].

Purification of synthesized nanoparticles

To remove the uncapped plant extract from the surface of the synthesized AuNPs and AgNPs, the nanoparticles were centrifuged at 10,000 rpm for 5 minutes. The supernatant liquid was decanted, and the nanoparticles were redispersed in distilled water; this process was repeated two more times. Finally, the obtained nanoparticles pellets were dispersed in distilled water. The *H. orixense*-mediated gold nanoparticles (HOAuNPs) and *H. orixense*-mediated silver nanoparticles (HOAgNPs) were dried in a hot air oven at 70°C to obtain a powder form [60].

Characterization of synthesized nanoparticles

UV-Visible spectroscopy

UV-visible spectroscopy is a widely accepted technique for determining the surface plasmon resonance (SPR) peak, which confirms the synthesis of AuNPs and AgNPs [61]. A double-beam spectrophotometer (UV-1800 Shimadzu UV-Spectrophotometer) was used to track the SPR peak after synthesis of the AuNPs and AgNPs. The absorbance was measured between 300 and 700 nanometres (nm) against distilled water as a blank [62].

Particle size and zeta potential

The particle size, size distribution, and zeta potential of the biologically synthesized AuNPs and AgNPs were determined using a particle size analyser/zeta potential analyser (Litesizer 500), where the average hydrodynamic diameter and mean zeta potential were measured [63].

Fourier transform infrared (FTIR) Spectroscopy

FTIR analysis was performed to examine the surface chemistry and identify the functional groups of AuNPs and AgNPs. The powdered AuNPs and AgNPs were positioned on the FTIR instrument's sample holder, and PerkinElmer Spectrum IR Version 10.7.2 was used to capture FTIR spectra in transmission mode between the 400 and 4000 cm^{-1} range [64].

X-Ray Diffraction (XRD)

The X-ray diffractometer (XRD) (Rigaku; Smart Lab 9KW) was used for phase identification, to determine the purity and nature of the biosynthesized AuNPs and AgNPs. The diffraction angle (2Θ) was changed in steps of 2° per minute, ranging from 20° to 80° [65].

Scanning electron microscopy (SEM)

The powder samples were subjected to microstructural studies using a scanning electron microscope (SEM) (JEOL® JSM-6390LV), which demonstrated the morphology of the samples. Images were captured at different magnifications to clearly show their properties [66].

Thermogravimetric analysis (TGA)

Thermogravimetric analysis (TGA) of synthesized AuNPs and AgNPs was conducted using a Shimadzu Corporation, DTG-60 TGA instrument within a controlled nitrogen environment. The samples were subjected to a temperature ramp from 30°C to 400°C at a constant heating rate of 10°C/min, allowing for the measurement of weight loss throughout the heating process, providing valuable insights into the thermal stability of the samples [67,68].

Biological activity

The biological activity of the extract and synthesized nanoparticles, including anticancer and antioxidant activities, was studied.

Antioxidant activity

The antioxidant activity was evaluated using a dot-blot method. Silica precoated HPTLC plates were used for real-time screening of antioxidant compounds present in the extract and nanoparticles. The extract and synthesized nanoparticles (10mg/mL) were applied to the plate, which was then developed in a mobile phase consisting of Toluene: Ethyl acetate: Formic acid: Methanol in the ratio of 6:6:1.6:0.4. The plate was dipped in a DPPH solution (0.4mmol/L), and areas with antioxidant compounds appeared as yellow spots or bands against a purple background, with the intensity of yellow colour correlating with antioxidant activity [67].

Anticancer activity

The anticancer activity of the extract and synthesized nanoparticles (HOEE, AuNP, and AgNP) was evaluated against three cancer cell lines at Biometrica lab, Ludhiana:

- Human Breast Cancer Cell Line Studies (MCF-7)
- Human Lung Cancer Cell Line Studies (A549)
- Human Liver Cancer Cell Line Studies (HepG2)

The culture medium was prepared using Dulbecco's Modified Eagle Medium (DMEM) from Gibco, supplemented with 10% Fetal Bovine Serum (FBS), penicillin (50 µg/mL), streptomycin (50 µg/mL), gentamicin (50 µg/mL), amphotericin B (2.5 µg/m, L-glutamine (1 mM), and non-essential amino acids. The prepared culture medium was placed in a humidified incubator set to maintain optimal conditions: Temperature: 37°C, Carbon Dioxide (CO_2) 5% to maintain pH stability of the medium. MCF-7 (breast cancer cells), A549 (lung carcinoma cells), and HepG2 (liver cancer cells) were thawed and revived using aseptic techniques, then added to the prepared culture medium and allowed to attach and grow in the incubator. The cells were regularly monitored and observed under a microscope to check for confluency, health, and any signs of contamination. When cells reached around 70-80% confluency (a dense monolayer covering the culture dish), they were subcultured: the old medium was aspirated, cells were washed with PBS (phosphate-buffered saline), detached using trypsin-EDTA solution, and neutralized with fresh culture medium containing FBS, which inhibits trypsin activity. The cells were transferred to new culture plates with fresh DMEM to ensure continued growth in optimal conditions.

For treatment, the cells were prepared as a monolayer in culture plates by allowing them to attach and grow until they reach the desired confluency. Once ready, the cells were exposed to varying concentrations of selected extracts by diluting the extracts in the culture medium. The treated cells were incubated in the 5% CO_2 incubator at 37°C for a 24-hour period, ensuring consistency across all samples for accurate results. After the 24-hour treatment period, the cells were analysed for various parameters, depending on the objectives of the study (e.g., cell viability, cytotoxicity,

morphological changes). The appropriate assays were used to quantify the effects of the extracts, following each assay's protocol meticulously to ensure reproducibility and accuracy [69].

Approximately 1×10^4 cells (MCF-7, HepG2, and A549) were seeded in each well of a 96-well plate specifically designed for cell culture. The plate was placed in a humidified incubator set at 37°C with 5% CO_2 to allow the cells to adhere and grow. Cell growth was monitored until reaching around 70% confluency. Once cells reach the desired confluency, a range of concentrations were prepared for the samples (HOEE, AuNP, and AgNP) to be tested. Different concentrations of each sample were added to the wells, ensuring consistent volume across all treatments. The 96-well plate was placed back in the incubator and the cells were exposed to the samples for a 24-hour period. After the 24-hour treatment, the treatment media was carefully aspirated and removed from each well. MTT (3-(4,5-Dimethylthiazol-2-yl)-2,5-Diphenyltetrazolium Bromide) solution was prepared at a concentration of 5 mg/mL in phosphate-buffered saline (PBS) [70]. An equal volume of MTT solution (typically 10-20 µL, depending on the assay protocol) was added to each well. The plate was returned to the incubator and the cells were allowed to react with MTT for 3 hours at 37°C. During this time, viable cells was converting the yellow MTT solution into purple formazan crystals. After the 3-hour incubation, the wells were observed for the presence of purple formazan crystals, which indicates cell viability. The MTT solution was carefully aspirated and a solubilizing agent, such as dimethyl sulfoxide (DMSO) or an acidified isopropanol solution, was added to each well [71]. This step dissolves the formazan crystals, creating a coloured solution. The 96-well plate were then placed in a microplate reader. The optical density (OD) of each well was measured at a wavelength of 570 nm, which corresponds to the absorbance of formazan. The OD values were recorded, as higher values correlate with higher cell viability. The percentage of viable cells were calculated in each treatment group by comparing the OD of treated wells to that of control wells (untreated cells) [72].

RESULTS AND DISCUSSION

Preliminary phytochemical screening

Phytochemical screening involved various chemical tests to confirm the presence of phytoconstituents in the extract.

The root bark extract tested positive for alkaloids, flavonoids, coumarins, tannins, quinones, carbohydrates, and phytosterols.

HPTLC profiling

HPTLC analysis was performed on the samples for fingerprinting purposes. The plates were

developed in a chamber, dried, and introduced to a visualizer for spot detection. Images were captured under three conditions after derivatization. Figure 7 shows the TLC plate images at 254nm, 366nm, and after derivatization under white light.

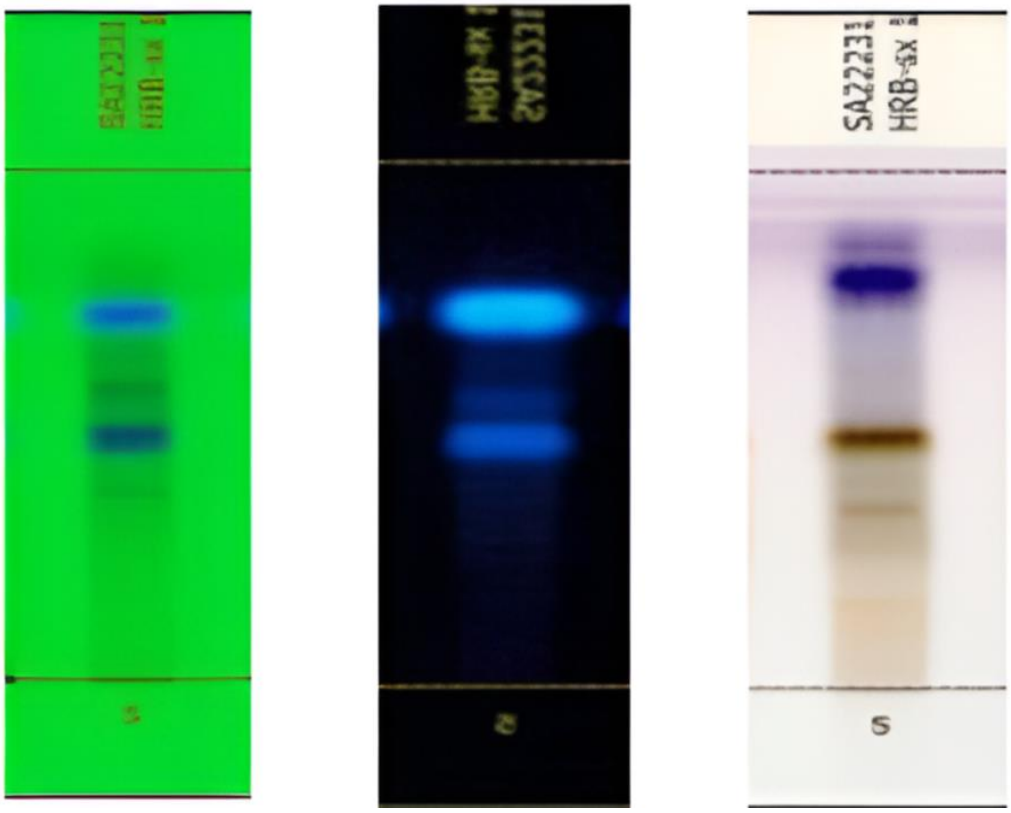

Figure 7: HPTLC chromatogram image at 254 nm, 366 nm, and white light after derivatization.

The observed bands in each image, along with their Rf values and colours are mentioned in Table 1 and graphically represented in Figure 8.

Table 1: Observed bands with Rf value and colour.

Image after development at R 254 nm		Image after derivatization at R white	
Rf value	**Colour**	**Rf value**	**Colour**
0.37	Blue	0.13	Cream
0.48	Blue	0.35	Light brown
0.57	Blue	0.49	Brown
0.71	Blue	0.79	Violet

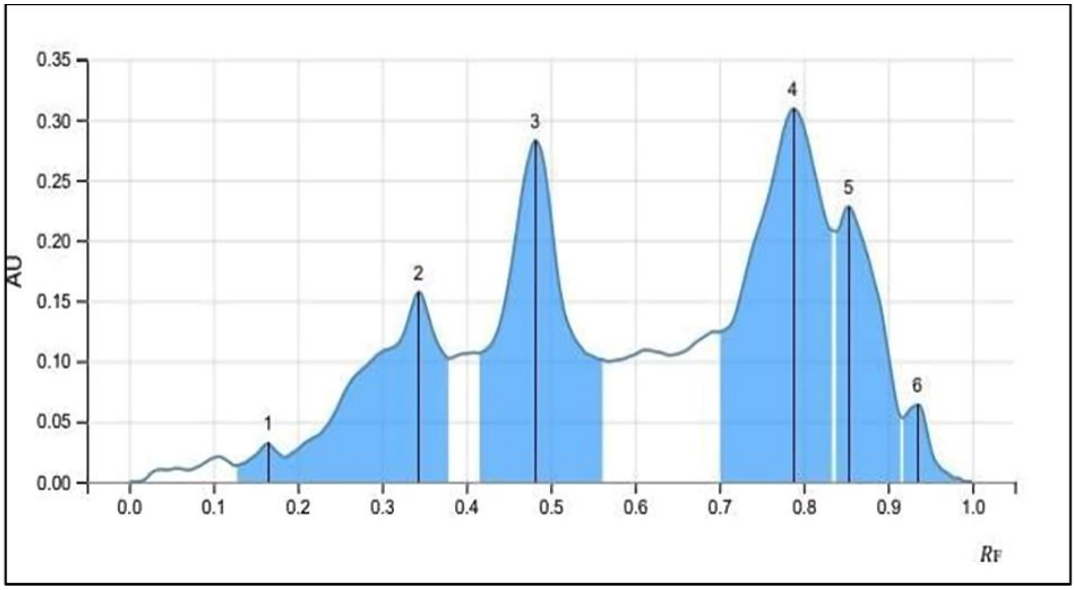

Figure 8: Graph representation by ethanolic extract of *H. orixense* root bark compound.

TLC studies

TLC was performed using Chloroform: Acetonitrile as the solvent system. Scopoletin emits blue fluorescence under ultraviolet irradiation at 366 nm and has a R_f value of around 0.75 in this solvent system [51].

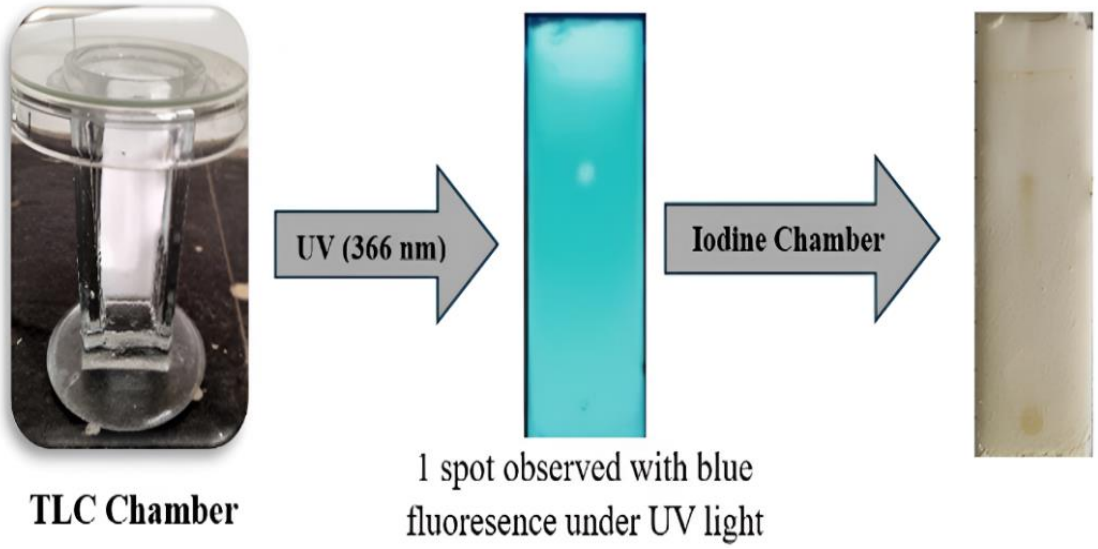

Figure 9: TLC of the extract observed in UV (366 nm) and iodine chamber.

A single spot was observed under UV light and in the iodine chamber, with R_f value of 0.74 as represented in Figure 9, confirming the presence of scopoletin, as per the literature value.

LC-MS

The HOEE compound was analyzed using ESI, and various compounds were identified, including (-)- jasmonoyl-L-isoleucine (catabolic pathway of the plant hormone jasmonate), glycosides, Isoleucyl- threonine (dipeptide), L-Alpha-glutamyl-L-hydroxyproline (Dipeptides), PC

(20:4(5Z,8Z,11Z,14Z)/P-18:1(11Z)). (Glycerophospholipid), Rheidin B (Anthracenes), Sarmentoloside (Cardenolide glycoside), Solamargine (cytotoxic compounds), scopoletin (coumarin derivative), scopoline (glucoside of scopoletin), and hymexelsin (apiose containing glycoside). The quantification results are mentioned in Table 2.

Table 2: Mass spectral characteristics and tentative identification of compounds present in the *Hymenodictyon orixense* root bark extract by ethanol Compound (HOEE) using LC-ESI / MS positive mode.

Peak number	RT(Min)	Molecular formula	Molecular weight	Error(ppm)	Ms/ms fragment Score
1.(-)-jasmonoyl-Lisoleucine	23.39	C18H29NO4	324.2153	-5.72	67.33
2. Glycosides	27.225	C29H44O12	607.2712	-1.87	74.63
3. Isoleucyl-threonine	15.381	C10H20N2O4	250.1761	0.28	73.87
4. L-Alpha-glutamyl-L-Hydroxyproline	14.513	C10H16N2O6	261.1084	1.3	98.91
5. PC(20:4(5Z,8Z,11Z, 14Z)/P-18:1(11Z)	10.46	C46H83NO7P	792.5926	3.5	58.37
6. Rheidin B	6.309	C30H20O8	509.1239	1.44	73.1
7. Sarmentoloside	26.409	C29H44O11	591.2763	-1.16	67.98
8. Solamargine	9.987	C45H73NO15	443.2707	2.62	58.67
9. Scopoletin	8.62	C10H8O4	193.0491	0.92	88.02
10. Scopolin	9.06	C16H18O9	355.1021	2.01	92.01
11. Hymexelsin	11.89	C16H18O9	509.1261	-1.65	77.46

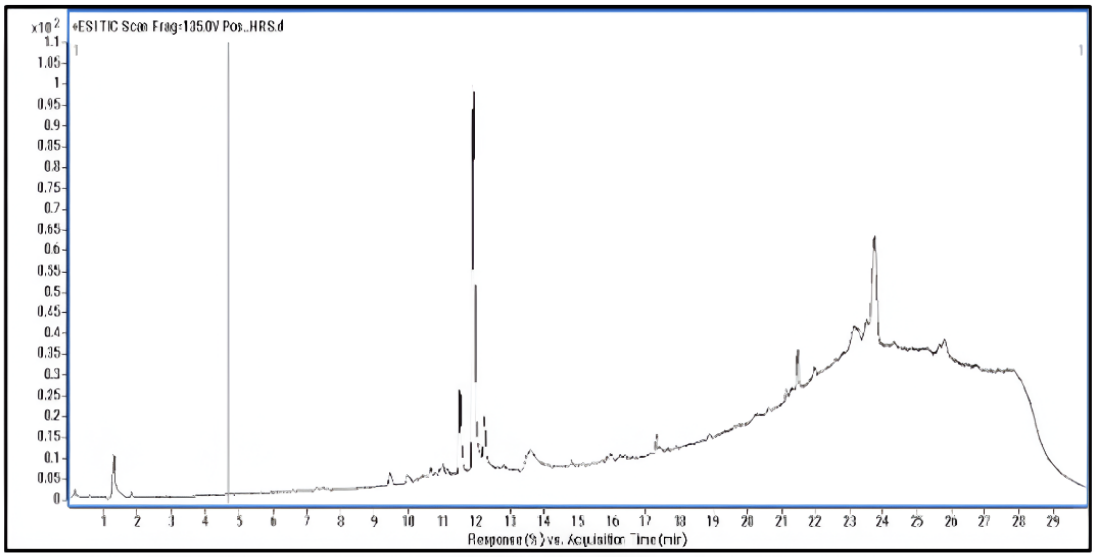

Figure 10: Mass spectral data compound present in the *Hymenodictyon orixense* root bark extract by ethanol compound (HOEE) using LC-ESI/ MS positive mode.

LCMS analysis in positive mode identified Scopolin (92.01%) as the most prominent compound, followed by Scopoletin (88.02%) and Hymexelsin (77.46%). The mass spectral data of LCMS is represented in Figure 10.

Quantitative analysis

The total phenolic content (TPC), total flavonoid content (TFC), and total tannin content (TTC) of *H. orixence* ethanolic extract were determined for quantitative analysis.The TPC was calculated from the gallic acid standard curve ($y = 0.0088x + 0.0072$, $R^2 = 0.9877$) and was found to be 14.48 mg GAE/g dried extract. The TFC was calculated from the quercetin standard curve ($y = 0.0006x + 0.001$, $R^2 = 0.9735$) and was found to be 290.83 mg QE/g dried extract, and the TTC was calculated from the tannic acid standard curve ($y = 0.0046x - 0.0077$, $R^2 = 0.9975$) and was found to be 310.43 mg TAE/g dried extract.

These secondary metabolites likely contribute to the extract's ability to reduce and synthesize HOAuNPs and HOAgNPs. Phenolics, flavonoids, and tannins are antioxidants that can degrade oxidizing chains and may directly affect antioxidative activity. They also serve as reducing agents and aid in nanoparticle synthesis, likely due to their presence on the surface of HOAuNPs and HOAgNPs.

Synthesis of gold and silver nanoparticles

The current work focuses on the rapid microwave-assisted synthesis of gold and silver nanoparticles using *H. orixense* root extract. The extract served as a reducing and stabilizing agent, evident from the colour change and absorption peaks in the UV-Vis spectra. Secondary metabolites like carbohydrates, amino acids, flavonoids, phenolics, and tannin groups in the root extract reduced metal ions, forming nanoparticles. Optimized conditions for the synthesis of gold and silver nanoparticles were determined by measuring the responses like hydrodynamic diameter and mean zeta potential of the synthesized AuNPs and AgNPs.

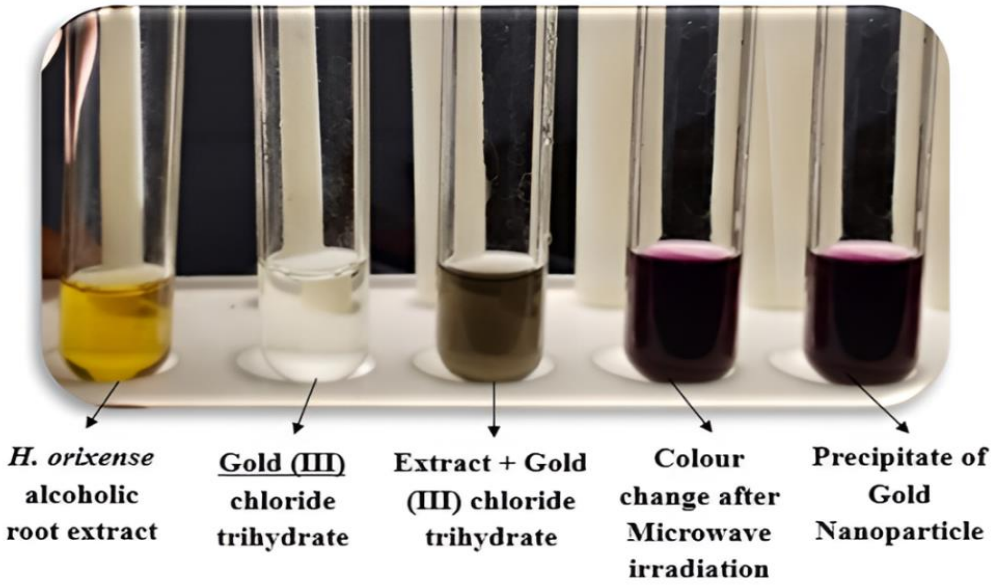

Figure 11: Visual observation of synthesis of gold nanoparticles.

For HOAuNPs, optimal conditions were: 480-watt microwave power, extract: metal salt solution (1 mM) in the ratio 1:9 (v/v), 90 seconds reaction time, resulting in a purple colour (Figure 11) and SPR peak at 544nm.

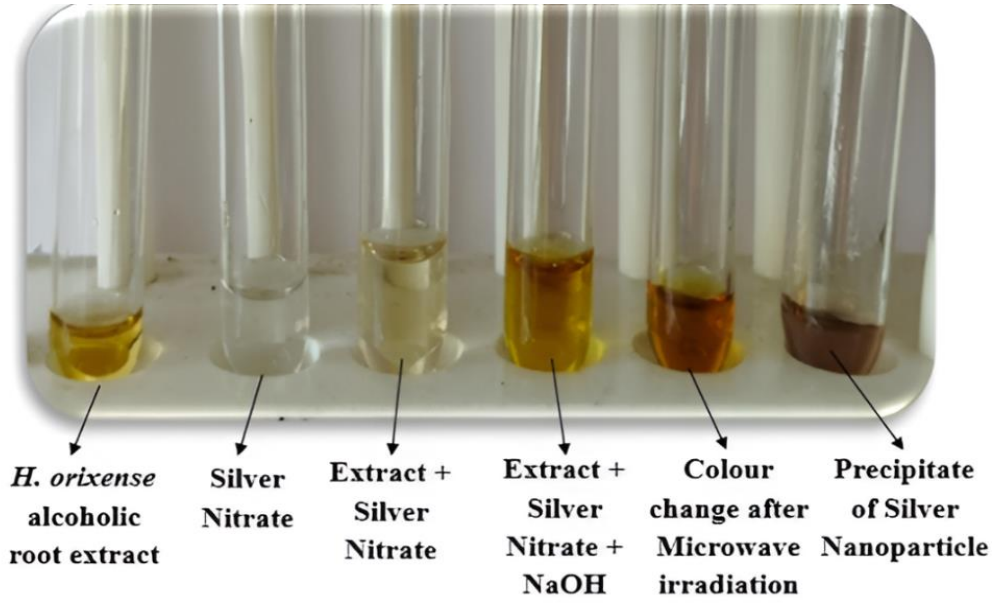

Figure 12: Visual observation of synthesis of silver nanoparticles.

For HOAgNPs, optimal conditions were: 800-watt microwave power, extract: metal salt solution (1 mM) in the ratio 1:9 (v/v), pH of the solution 8 (0.01 M NaOH), and 5-minute reaction time, resulting in a dark brown colour (Figure 12) and SPR peak at 427nm.

Characterization of synthesized nanoparticles

Synthesized nanoparticles were characterized using various physicochemical techniques.

UV Visible spectroscopy

UV-Visible spectroscopy revealed the surface plasmonic resonance (SPR) of the synthesized nanoparticles, which can be found by analysing the absorbance data.

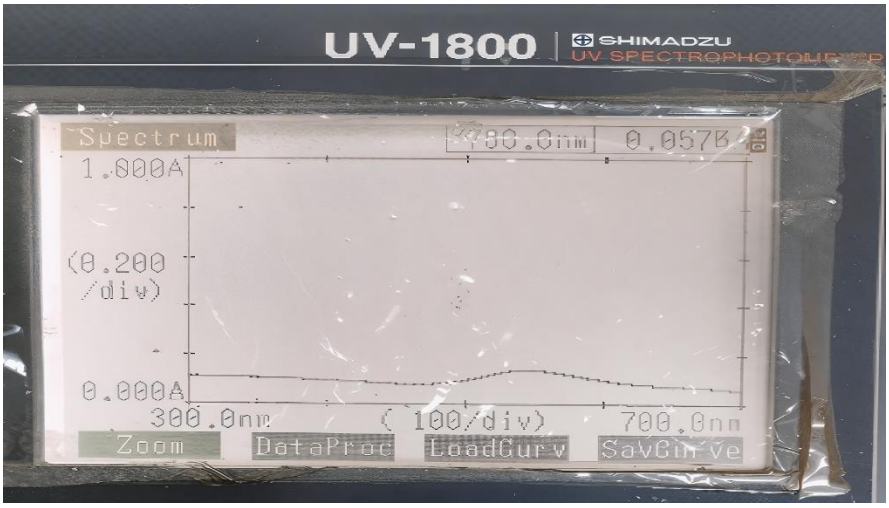

Figure 13: UV-Vis. Spectra of *H. orixense* AuNPs.

The SPR absorption of synthesized HOAuNPs showed a distinctive peak between 500 and 600 nm, confirming AuNPs formation. The optimised (Extract: Gold salt) 1:9 ratio resulted in a purple colour and SPR peak at 544 nm as represented in Figure 13. The SPR absorption of synthesised HOAgNPs showed a distinctive peak between 400 and 500 nm, confirming AgNPs formation. The optimised (Extract: Silver salt) 1:9 ratio resulted in a dark brown colour and SPR peak at 427 nm as represented in Figure 14.

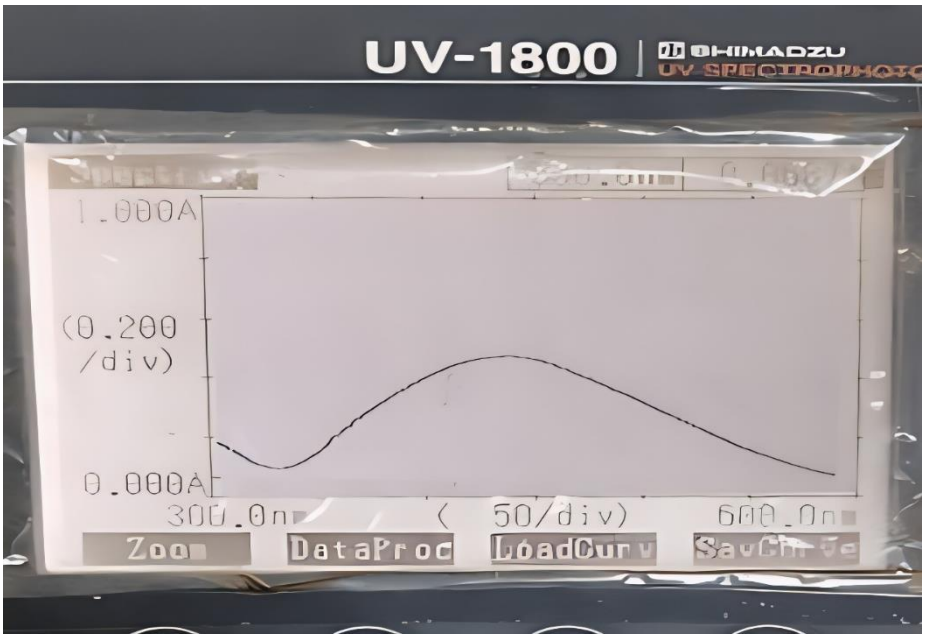

Figure 14: UV-Vis. Spectra of *H. orixense* AgNPs.

Particle size and zeta potential

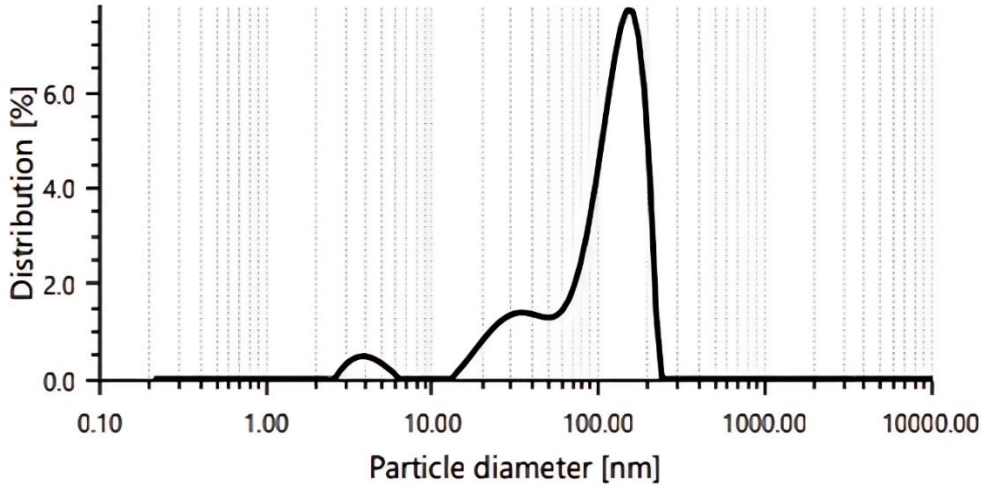

Figure 15: Particle size and size distribution of *H. orixense* AuNPs.

The dynamic light scattering analysis was used to determine the hydrodynamic diameter, polydispersity index (PDI), and zeta potential of biogenic AuNPs and AgNPs.

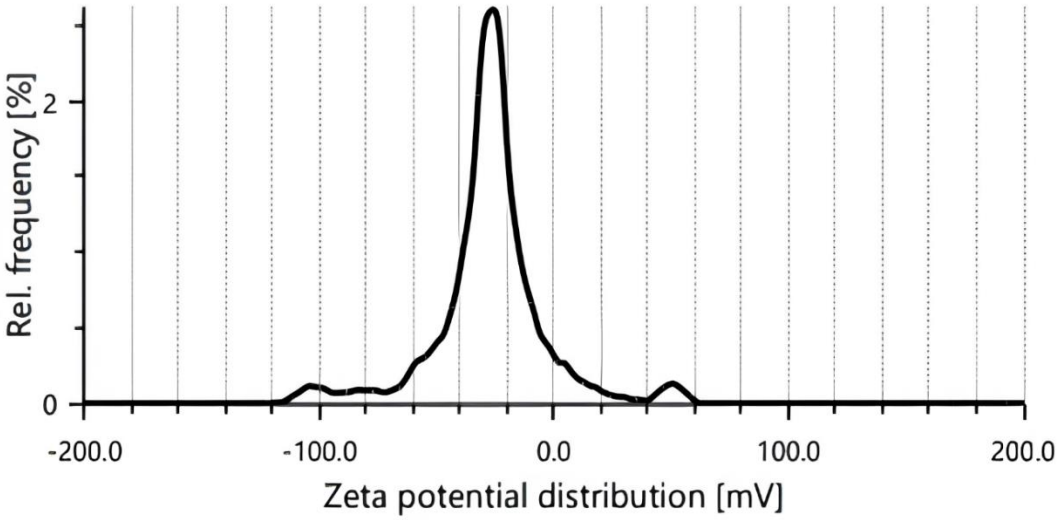

Figure 16: Zeta potential of *H. orixense* AuNPs.

The optimized HOAuNPs had a hydrodynamic diameter of 146.12 nm as represented in Figure 15, which was lower than that of other produced HOAuNPs. The optimised HOAuNPs had a PDI of 34.6%, and an average negative zeta potential of -29.1 mV as represented in Figure 16. Nanoparticles having zeta potentials ranging from -30 to +30 mV are stable and do not agglomerate in solution. As a result, the AuNPs are stable in solution. Electrostatic repulsion between NPs prevents aggregation due to high surface charge.

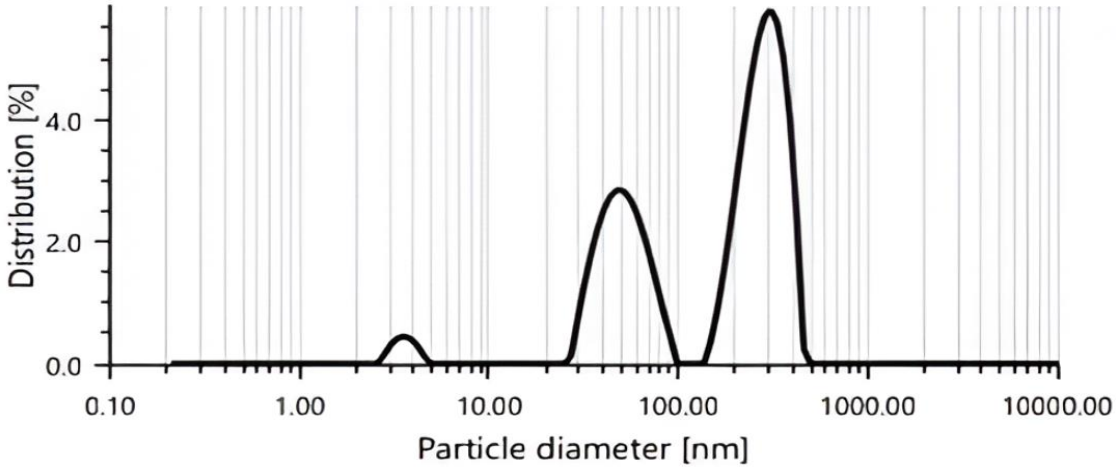

Figure 17: Particle size and size distribution of *H. orixense* AgNP.

The optimised HOAgNPs had a hydrodynamic diameter of 216.4 nm as represented in Figure 17, which was lower than that of other produced HOAgNPs. The optimised HOAgNPs had a PDI of 35.0%, and an average negative zeta potential of -27.2 mV as represented in Figure 18. As a result, the AgNPs are stable in solution.

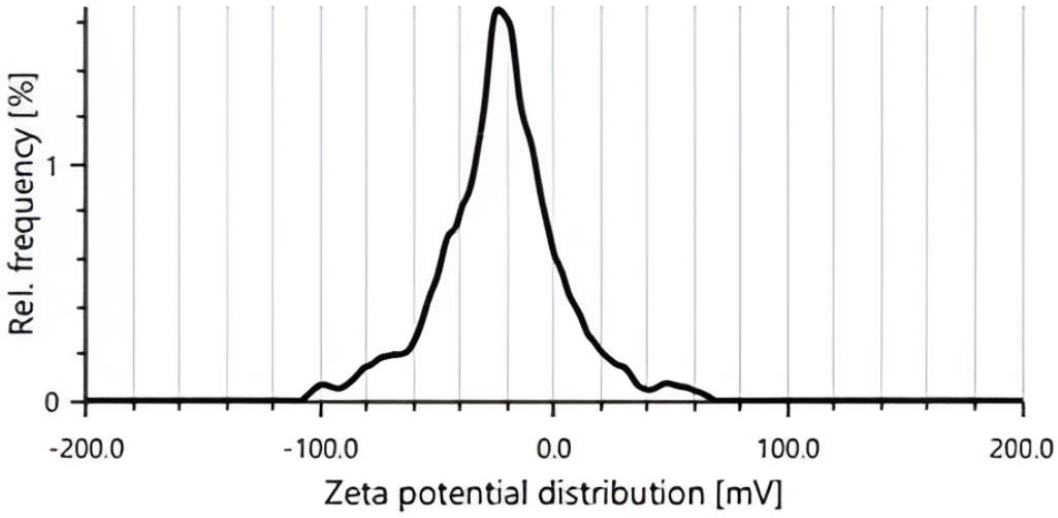

Figure 18: Zeta potential of *H. orixense* AgNPs.

The synthesized nanoparticles showed moderate polydispersity (PDI: 0.34-0.35), indicating potential aggregation or synthesis reproducibility issues. This may be attributed to variations in the phytochemical composition of the extract or optimization of synthesis parameters. The moderate polydispersity of the nanoparticles may impact their stability and bioactivity. Further optimization of synthesis parameters, such as extract concentration, salt ratio, and microwave power, may help improve the reproducibility and stability of the nanoparticles.

FTIR spectroscopy

The FTIR analysis of gold nanoparticles (HOAuNPs), silver nanoparticles (HOAgNPs), and *H. orixense* extract (HOEE) revealed key functional groups involved in the synthesis process.

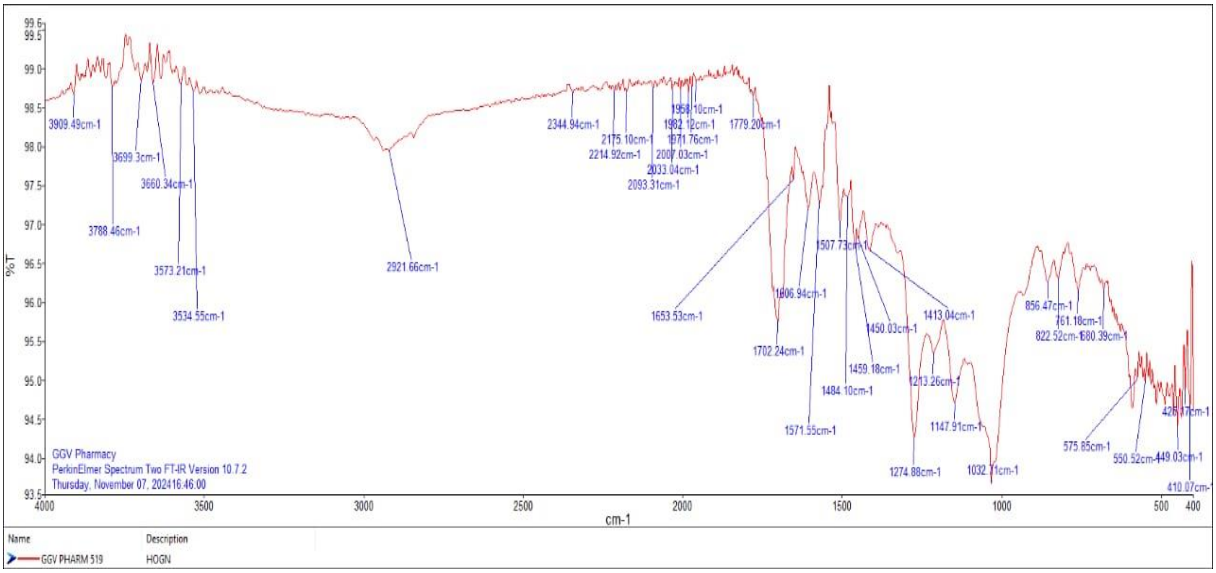

Figure 19: IR spectrum of gold nanoparticle.

The FTIR spectra of optimised HOAuNPs showed intense peak at 2921.66, 1702.24, 1274.88, 1147.91, and 1032.11 cm^{-1} as represented in Figure 19. The absorption band at 2921.66 cm^{-1} was due to the C-H stretching of the methylene group such as alkanes, alkenes, and alkynes. The presence of 1702.24 cm^{-1} peak was due to the presence of C=O stretching. The presence of 1274.88 cm^{1} was due to OH bending. The absorbance peak at 1147.91 cm^{-1} was due to the C-O stretching of primary alcohol group. The presence of 1032.11 cm^{-1} was due to C-O stretching. The result was portrayed in Table 3. These peaks were quite similar with the peaks found in FTIR spectra of HOEE as represented in Figure 20, which indicates the involvement of different biomolecules of HOEE in the synthesis of HOAuNPs. The result of HOEE was portrayed in Table 4.

Table 3: FTIR interpretation of gold nanoparticle.

S.No.	Wave No.	Functional group
1	2921.66	-C-H stretch
2	1702.24	-C=O (sharp)
3	1274.88	-OH bending (sharp)
4	1147.91	-C-O (CH_2OH) stretch (Primary alcohol)
5	1032.11	-C-O stretch

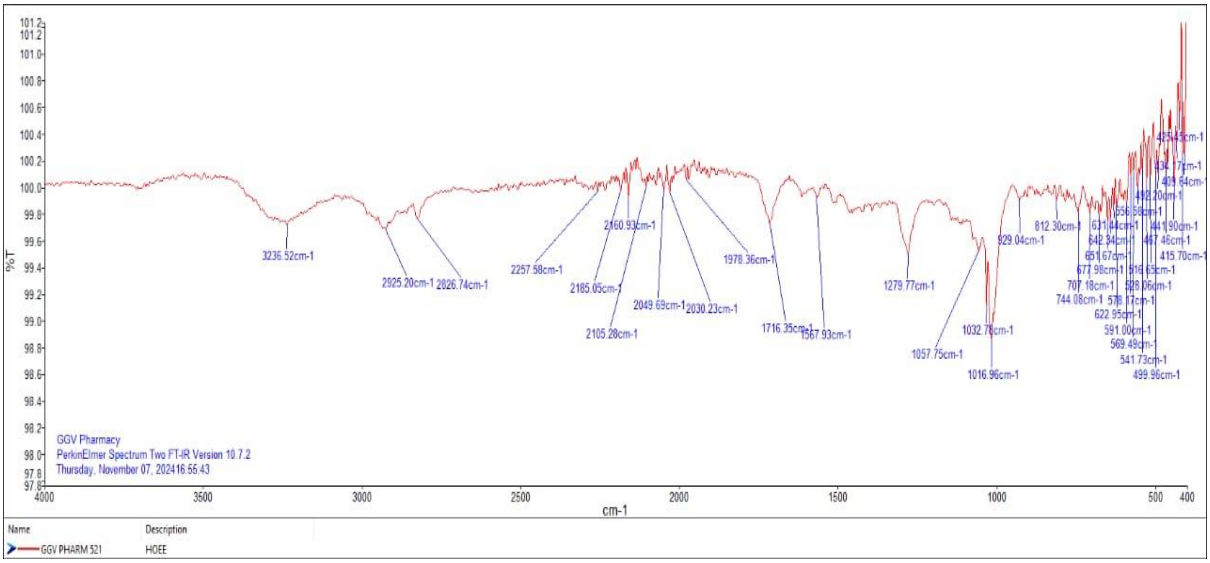

Figure 20: IR spectrum of *H. orixense* extract.

Table 4: FTIR interpretation of *H. orixense* extract.

S.No.	Wave No.	Functional group
1	3236.52	-OH stretch (broad)
2	2925.20	-C-H stretch
3	2826.74	-C-H stretch
4	1716.35	-C=O stretch
5	1279.77	-OH bending (sharp)
6	1016.96	-C-O stretch

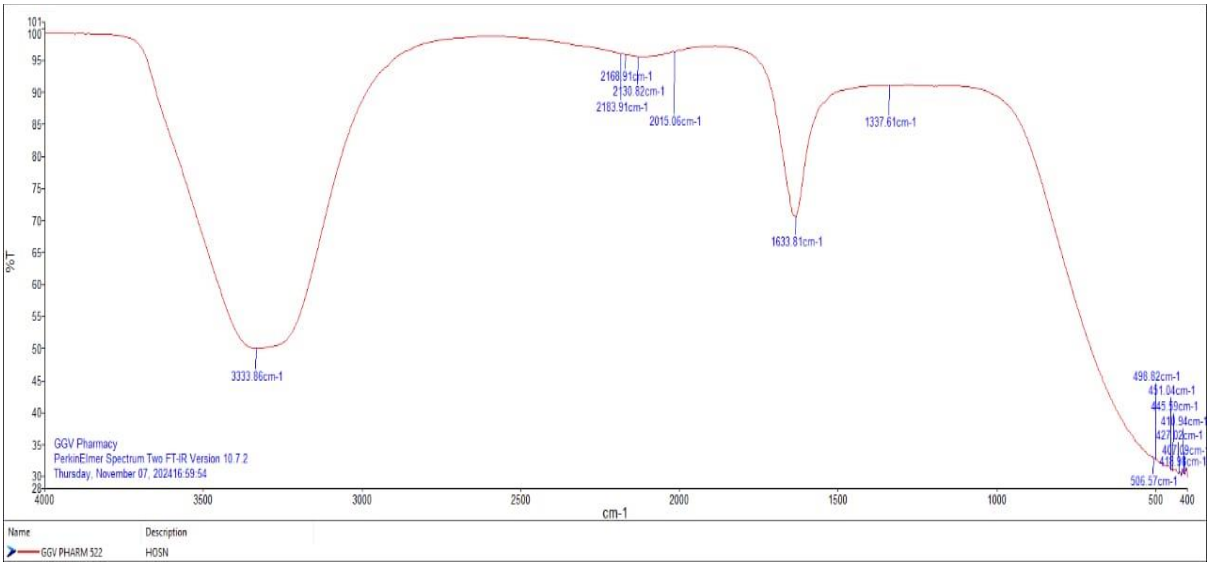

Figure 21: IR spectrum of silver nanoparticle.

Table 5: FTIR interpretation of silver nanoparticle.

S.No.	Wave No.	Functional group
1	3333.86	-OH stretch
2	1633.81	-OH bending

The FTIR spectra of optimised HOAgNPs showed intense peak at 3333.86 and 1633.81 cm^{-1} as represented in Figure 21. The broad peaks at 3333.86 cm^{-1} were obtained due to the -OH stretching of alcohol group. The presence of 1633.81 cm^{1} was due to the -OH bending [73]. The result was portrayed in Table 5. These peaks were quite similar with the peaks found in FTIR spectra of HOEE, which indicates the involvement of different biomolecules of HOEE in the synthesis of HOAgNPs.

The similarities between HOEE and nanoparticle FTIR spectra suggest biomolecules like phenolics, flavonoid, tannins, amino acids, and carbohydrates played a role in reducing, capping, and stabilizing metal ions during the synthesis. These chemical compounds were also identified by preliminary phytochemical screening of HOEE.

XRD analysis

The crystalline nature of synthesized gold and silver nanoparticles were determined by diffraction pattern obtained from XRD spectroscopy.

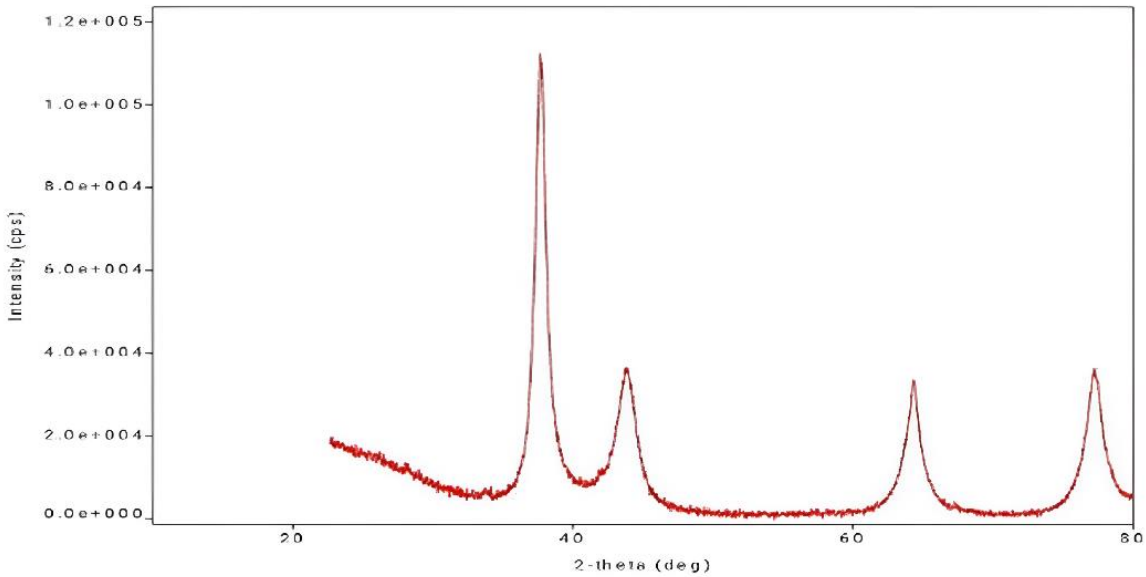

Figure 22: XRD pattern of biosynthesized *H. orixense* AuNPs by XRD-spectroscopy.

Table 6: XRD data of gold nanoparticle.

S.No.	2-theta (deg.)	Height (cps)
1	21.65	12556
2	37.685	72862
3	43.843	22610
4	64.306	21310
5	77.178	23773

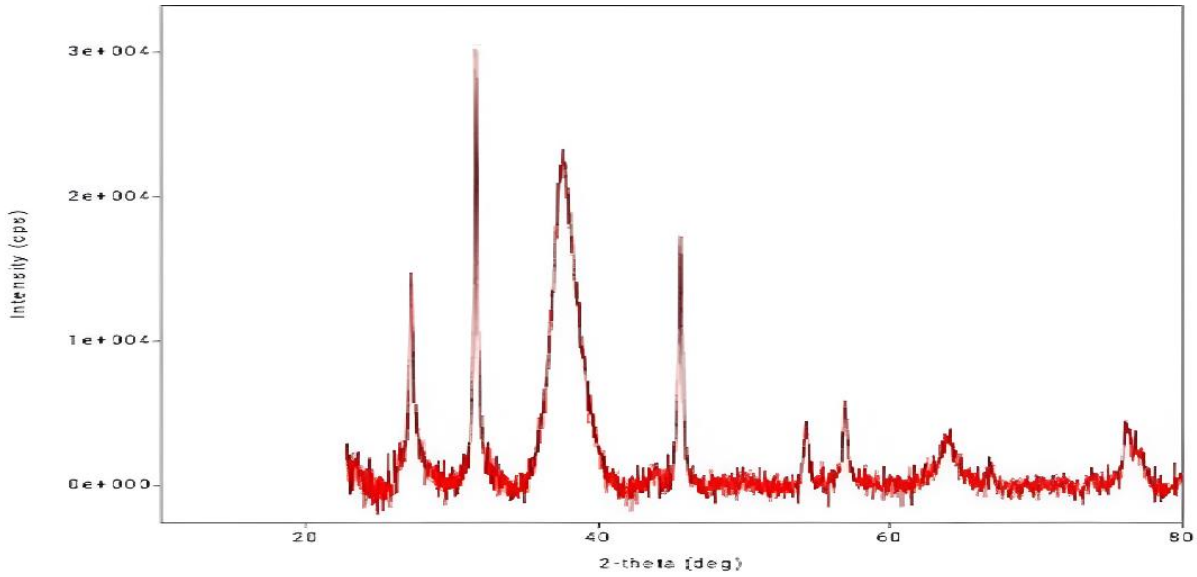

Figure 23: XRD pattern of biosynthesized *H. orixense* AgNPs by XRD-spectroscopy.

Table 7: XRD data of silver nanoparticle.

S.No.	2-theta (deg.)	Height (cps)
1	19.54	1777
2	27.162	9534
3	31.589	21859

4	37.515	13605
5	45.609	12741
6	54.22	2894
7	56.877	4054
8	63.74	2128
9	66.905	1085
10	76.225	2218

Gold nanoparticles showed diffraction peaks located at 37.68º, 43.84º, 64.30º, and 77.17º, as represented in Figure 22, corresponding to the (111), (200), (220), and (311) lattice planes, respectively, indicating a face-centered cubic (FCC) crystalline nature. XRD data of gold NPs was mentioned in Table 6.

Silver nanoparticles showed diffraction peaks located at 37.51º, 45.60º, 66.90º, and 76.22º, as represented in Figure 23, corresponding to the (111), (200), (220), and (311) lattice planes, respectively, also indicating a face-centered cubic (FCC) crystalline nature [74]. XRD data of silver NPs was mentioned in Table 7.

Scanning electron microscopy (SEM)

SEM analysis confirmed the shape and surface nature of biogenic AuNPs and AgNPs.

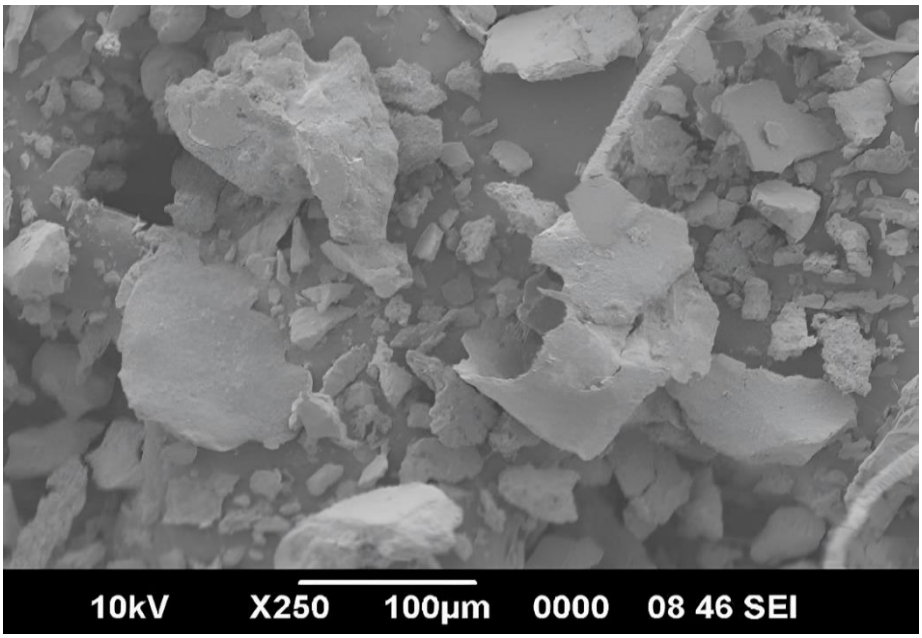

Figure 24: SEM images of Gold Nanoparticle.

Gold nanoparticles were spherical and irregularly shaped, with some aggregation likely due to the long incubation period (Figure 24). Silver nanoparticles were rod-like and irregularly shaped, also showing signs of aggregation (Figure 25) [66].

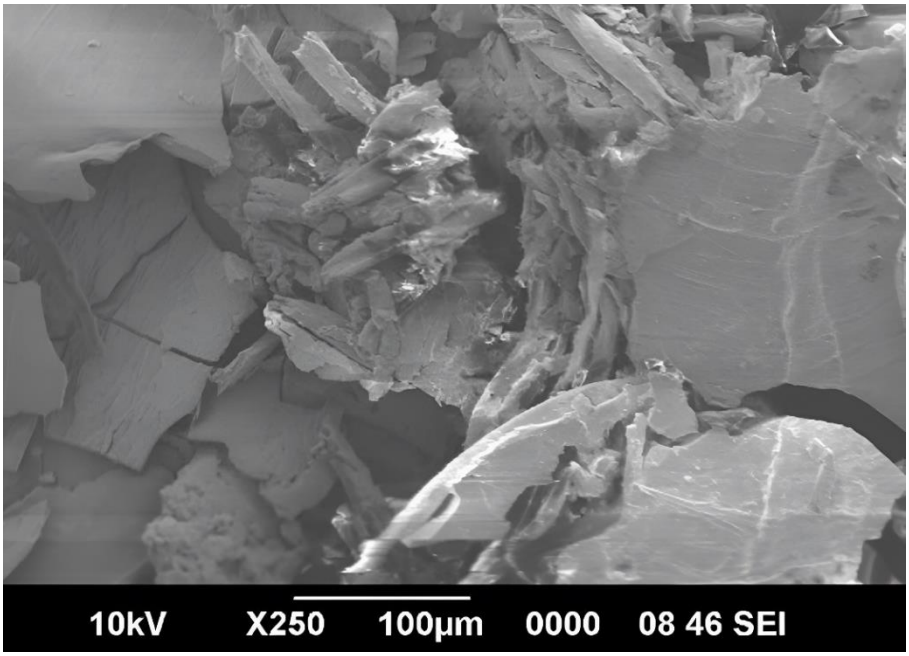

Figure 25: SEM images of Silver Nanoparticle.

Thermogravimetric analysis (TGA)

TGA analysis evaluated the thermal stability of synthesized gold and silver nanoparticles.

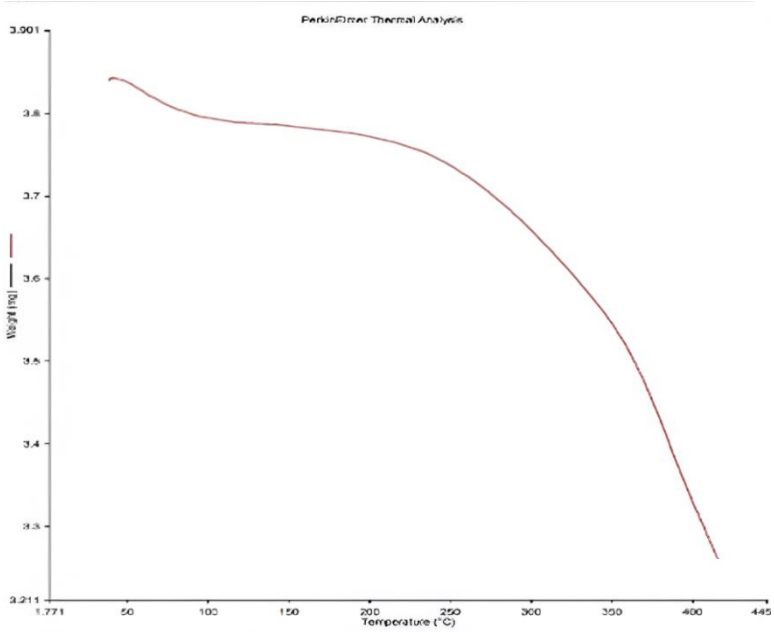

Figure 26: TGA curve of Gold Nanoparticle.

Gold nanoparticles showed a 15.97% weight loss when heated from a temperature ramp of 30℃ to 400℃, at a constant heating rate of 10℃/min, with an initial weight of 3.88mg and a final weight of 3.26 mg (Figure 26).

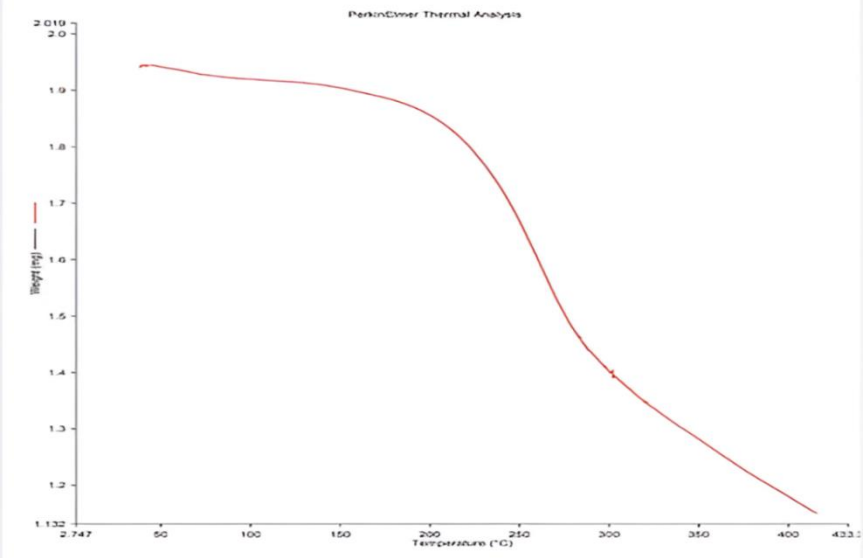

Figure 27: TGA curve of Silver Nanoparticle.

Silver nanoparticle showed a 41.02% weight loss when heated from a temperature ramp of 30℃ to 400℃, at a constant heating rate of 10℃/min, with an initial weight of 1.95 mg and a final weight of 1.15 mg (Figure 27).

Biological activity

Invitro anticancer and antioxidant study of extract and synthesized nanoparticles were studied.

Antioxidant activity

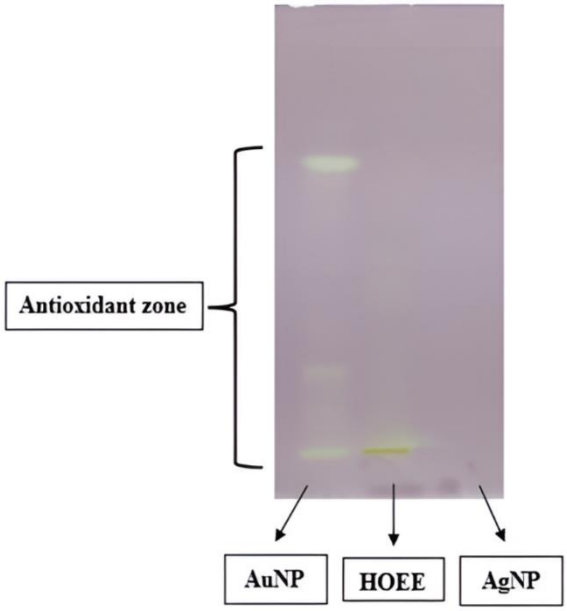

Figure 28: Comparison of antioxidant activity by using dot-blot method.

The dot-blot analysis evaluated the *Invitro* antioxidant activity of the extract and synthesized nanoparticle (Figure 28). Gold nanoparticles showed more intense yellow spots compared to the extract and silver nanoparticles, indicating that gold nanoparticle shows significant antioxidant

activity. The intensity of yellow bands or spots directly correlates with the antioxidant activity, as the DPPH solution (0.4mmol/L) stains the plate purple, and areas with antioxidant compounds appear as yellow spots or bands [67]

Anticancer activity

The *invitro* anticancer activity of biosynthesized gold and silver nanoparticles was evaluated against breast cancer MCF-7, lung cancer A549, and liver cancer HepG2 cell lines using MTT assay. Morphological changes in breast cancer MCF-7, lung cancer A549, and liver cancer HepG2 cell line at 1000 µg/mL were observed, when the samples were introduced, as represented in Figure 29.

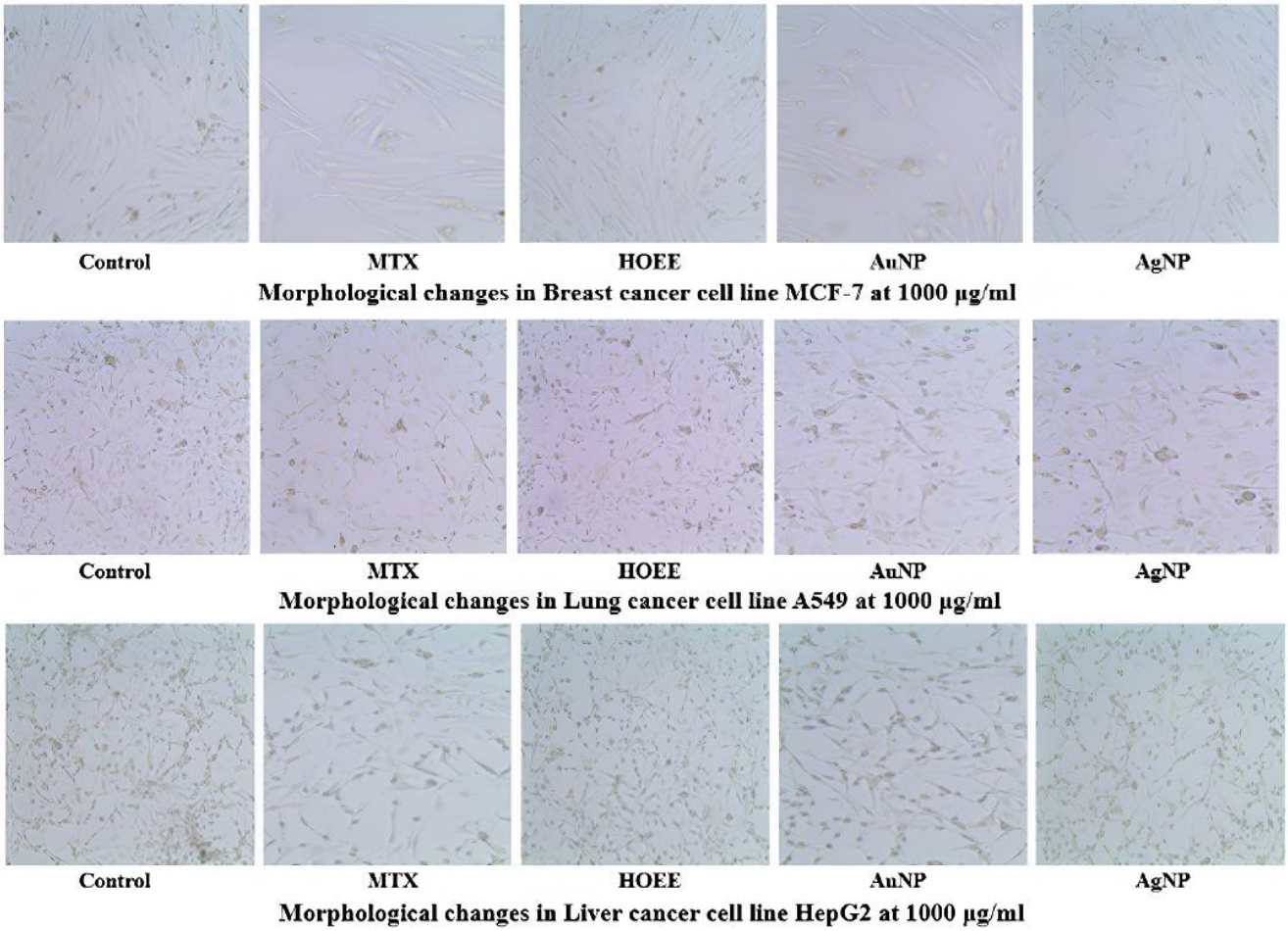

Figure 29: Morphological changes in MCF-7, A549, and HepG2 cancer cell line at 1000 µg/mL.

In Figure 30, 31, and 32, a bar graph depicting the effectiveness of biosynthesized gold and silver nanoparticles against MCF7, A549, and HepG2 cells at various concentrations (10, 50, 100, 200, 400, 800, and 1000 µg/mL) was displayed.

Gold nanoparticles showed potent cytotoxic activity with IC_{50} values of 291.23, 306.31, and 556.1 µg/mL against MCF-7, A549, and HepG2 respectively. Silver nanoparticles showed IC_{50} values of

372.59, 581.70, and 575.31 µg/mL against MCF-7, A549, and HepG2 respectively (Table 8, 9, 10).

Both nanoparticles demonstrated dose-dependent cytotoxicity, with both gold and silver nanoparticles showing higher activity against MCF-7 compared to other cell lines. The synthesized nanoparticles likely exert their anticancer effects through ROS generation and apoptosis induction, as suggested by previous studies on plant-mediated nanoparticles [75].

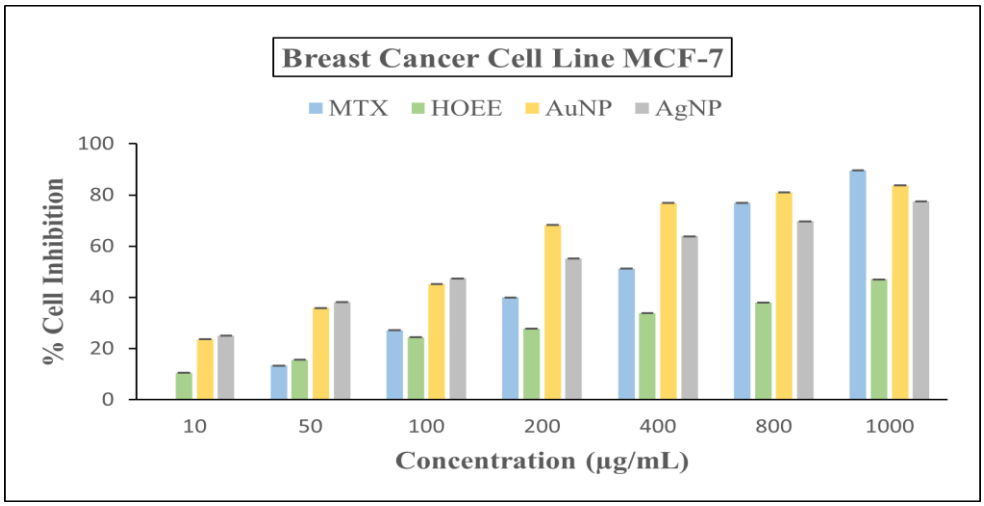

Figure 30: Graph showing %cell inhibition: Human Breast Cancer Cell Line MCF-7.

Table 8: Representing IC_{50} and cell viability (at 1000 µg/mL) of samples in MCF-7 cell line.

Sample	IC_{50} (µg/mL)	Cell Viability (%)
Methotrexate (MTX) (Standard)	440.64	10.31%
H. orixense extract (HOEE)	1034.42	52.93%
Gold nanoparticle (AuNP)	291.23	16.19%
Silver nanoparticle (AgNP)	372.59	22.48%

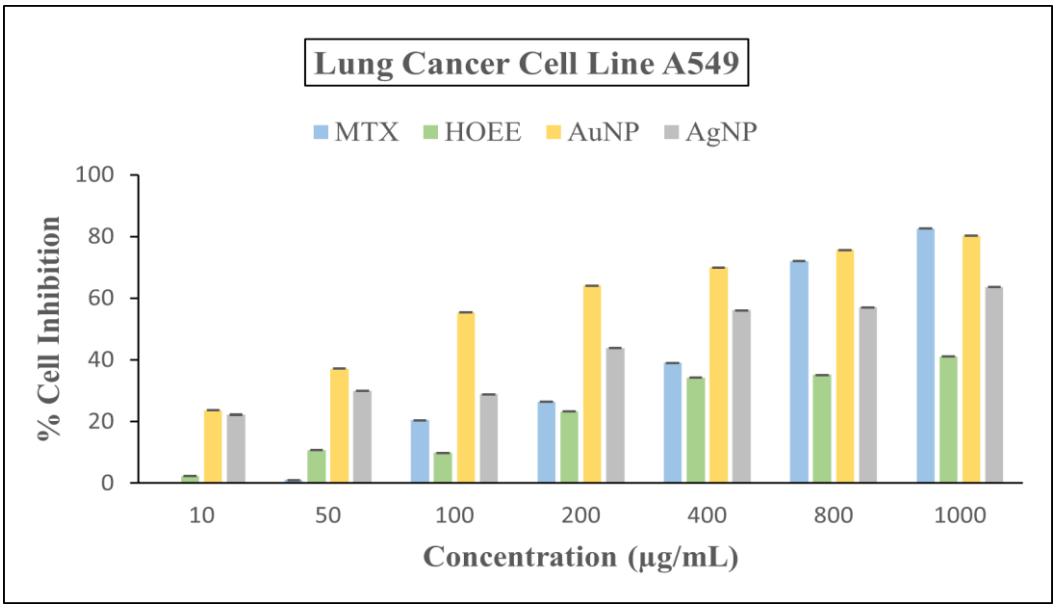

Figure 31: Graph showing %cell inhibition: Human Lung Cancer Cell Line A549.

Table 9: Representing IC_{50} and cell viability (at 1000 µg/mL) of samples in A549 cell line.

Sample	IC_{50} (µg/mL)	Cell Viability (%)
Methotrexate (MTX) (Standard)	553.77	13.91%
H. orixense extract (HOEE)	1126.28	58.89%
Gold nanoparticle (AuNP)	306.31	19.73%
Silver nanoparticle (AgNP)	581.70	36.34%

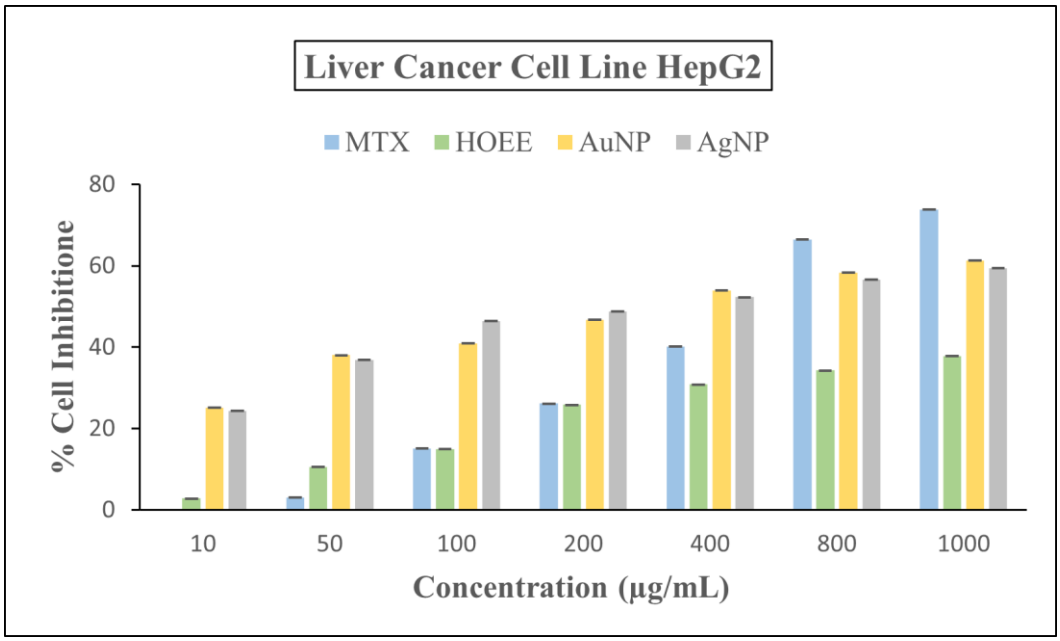

Figure 32: Graph showing %cell inhibition: Human Liver Cancer Cell Line HepG2.

Table 10: Representing IC_{50} and cell viability (at 1000 µg/mL) of samples in HepG2 cell line.

Sample	IC_{50} (µg/mL)	Cell Viability (%)
Methotrexate (MTX) (Standard)	599.30	26.17%
H. orixense extract (HOEE)	1228.02	62.20%
Gold nanoparticle (AuNP)	556.1	38.71%
Silver nanoparticle (AgNP)	575.31	40.59%

The experiments were executed in three replicates (n = 3). The data were analyzed by two-way ANOVA and statistical difference between test samples was analyzed. The *P-value ≤ 0.001 were considered significant.

A dose-related reduction in viable cells was reported after a 24-hr treatment of MCF-7, A549, and HepG2 with varied concentrations of *H. orixense* inspired gold and silver nanoparticles. Based on these results, the IC_{50} were determined. The IC_{50} values of the AuNPs and AgNP were lower than that of the *H. orixense* root extract (>1000 µg/mL), against MCF-7, A549, and HepG2 cell lines. At 1000 µg/mL, gold nanoparticles killed 83.81%, 80.27%, and 61.29% of MCF-7, A549, and HepG2 cells, respectively, while silver nanoparticles killed 77.52%, 63.66%, and 59.41% of MCF-7, A549, and HepG2 cells, respectively.

CONCLUSION

The present research study highlights the extraction, phytochemical screening, and microwave-assisted green synthesis of gold and silver nanoparticles using the alcoholic root extract of *Hymenodictyon orixense*, as well as the investigation of the anticancer and antioxidant activities of the extract and synthesized nanoparticles. The use of *Hymenodictyon orixense* root extract for the green synthesis of gold and silver nanoparticles offers a novel, eco-friendly, and cost-effective approach. Compared to other plant-based synthesis methods, *H. orixense* extract provides a unique combination of phytochemicals that act as reducing and stabilizing agents, resulting in nanoparticles with significant anticancer and antioxidant activities. The synthesized nanoparticles showed potent cytotoxicity against MCF-7, A549, and HepG2 cancer cell lines, with IC_{50} values indicating promising anticancer potential. Notably, gold nanoparticles exhibited higher anticancer and antioxidant activity than the extract and silver nanoparticles.

While these findings are encouraging, it's essential to acknowledge that in vivo validation and mechanistic studies are necessary to fully understand the therapeutic potential of these nanoparticles. Additionally, further research is needed to assess the anticancer activity of various extracts and fractions of *H. orixense*. Moving forward, exploring targeted delivery, combination therapies, and toxicity assessments in normal cells could provide valuable insights into the biomedical applications of these nanoparticles. The eco-friendly synthesis and promising bioactivity of *H. orixense*-derived nanoparticles make them an attractive candidate for future drug development and cancer therapy research.

ACKNOWLEDGEMENT

The authors would like to extend sincere gratitude to Guru Ghasidas University for providing a conductive research environment and facilities. The authors are thankful to Dr. Rishi Paliwal, Associate Professor, Department of Pharmacy, Indira Gandhi National Tribal University, and Dr. J. Venkatesan, Professor, Birla Institute of Technology, Mesra, Ranchi for their support in characterization of nanoparticles and providing the results of the same. The authors are equally thankful to Dr. Tushar Gupta and team, Biometrica, Ludhiana for providing the anticancer report of samples.

REFERENCES

1. Schmidt C, Storsberg J. Nanomaterials-tools, technology and methodology of nanotechnology based biomedical systems for diagnostics and therapy. Biomedicines 2015;3:203–23. https://doi.org/10.3390/biomedicines3030203.

2. Pawelski D, Plonska-Brzezinska ME. Microwave-Assisted Synthesis as a Promising Tool for the Preparation of Materials Containing Defective Carbon Nanostructures: Implications on Properties and Applications. Materials 2023;16. https://doi.org/10.3390/ma16196549.
3. Moghimi SM, Hunter AC, Murray JC. Nanomedicine: current status and future prospects. The FASEB Journal 2005;19:311–30. https://doi.org/10.1096/fj.04-2747rev.
4. Adeyemi JO, Oriola AO, Onwudiwe DC, Oyedeji AO. Plant Extracts Mediated Metal-Based Nanoparticles: Synthesis and Biological Applications. Biomolecules 2022;12. https://doi.org/10.3390/biom12050627.
5. Mohamad Sukri SNA, Shameli K, Teow SY, Chew J, Ooi LT, Lee-Kiun Soon M, Ismail NA, Moeini H. Enhanced antibacterial and anticancer activities of plant extract mediated green synthesized zinc oxide-silver nanoparticles. Front Microbiol 2023;14. https://doi.org/10.3389/fmicb.2023.1194292.
6. Dubey S, Virmani T, Yadav SK, Sharma A, Kumar G, Alhalmi A. Breaking Barriers in Eco-Friendly Synthesis of Plant-Mediated Metal/Metal Oxide/Bimetallic Nanoparticles: Antibacterial, Anticancer, Mechanism Elucidation, and Versatile Utilizations. J Nanomater 2024;2024. https://doi.org/10.1155/2024/9914079.
7. Reddy KTK, Dharmamoorthy G, Devi DV, Vidiyala N, Bagade OM, Elumalai S, Dantinapalli VLS, Kasimedu S. Phytoconstituent-Based Green Synthesis of Nanoparticles: Sources and Biomedical Applications in Cancer Therapy. Asian Journal of Green Chemistry 2025;9:329–54. https://doi.org/10.48309/AJGC.2025.501113.1669.
8. Kumar P, Kumar S, Tapwal A, Nimesh S, Thakur N. Water purification and biological efficacy of green synthesized Co/Zn-Doped α-Fe2O3 nanoparticles. Sustainable Chemistry for the Environment 2024;8. https://doi.org/10.1016/j.scenv.2024.100160.
9. Adeola AO, Duarte MP, Naccache R. Microwave-assisted synthesis of carbon-based nanomaterials from biobased resources for water treatment applications: emerging trends and prospects. Frontiers in Carbon 2023;2. https://doi.org/10.3389/frcrb.2023.1220021.
10. Patil A, Phole PM, Charde MS, Chakole RD, Mali N, Balasaheb Patil A. Microwave assisted organic synthesis: a green chemistry approach 1. vol. 8. 2023.
11. Kustov L, Vikanova K. Synthesis of Metal Nanoparticles under Microwave Irradiation: Get Much with Less Energy. Metals (Basel) 2023;13. https://doi.org/10.3390/met13101714.
12. Ritu, Verma KK, Das A, Chandra P. Phytochemical-Based Synthesis of Silver Nanoparticle: Mechanism and Potential Applications. Bionanoscience 2023;13:1359–80. https://doi.org/10.1007/s12668-023-01125-x.

13. Soliman MKY, Talib AH, Mahmoud R, Ali ZA, Al-Haideri HH, Abalkhail A, Binshaya AS, Salem MH, Al-Otibi FO, Yassin MT. Ecofriendly magnesium oxide nanoparticles: anticancer, antimicrobial, and antidiabetic potentials in vitro. AMB Express 2025;15:143. https://doi.org/10.1186/s13568-025-01950-1.
14. Patil MD. Plant Mediated Nanoparticle Synthesis, Characterization and its Applications in Various Fields: A Review. n.d.
15. Freitas DC, Mazali IO, Sigoli FA, da Silva Francischini D, Arruda MAZ. The microwave-assisted synthesis of silica nanoparticles and their applications in a soy plant culture. RSC Adv 2023;13:27648–56. https://doi.org/10.1039/d3ra05648a.
16. Raju SK, Sekar P, Kumar S, Murugesan M, Karthikeyan M. Plant-Mediated Green Synthesis of Gold Nanoparticles and Their Anticancer Applications: An Updated Review. Journal of Applied Pharmaceutical Sciences and Research 2022;4:1–20. https://doi.org/10.31069/japsr.v4i4.1.
17. Stozhko N, Tarasov A, Tamoshenko V, Bukharinova M, Khamzina E, Kolotygina V. Green Silver Nanoparticles: Plant-Extract-Mediated Synthesis, Optical and Electrochemical Properties. Physchem 2024;4:402–19. https://doi.org/10.3390/physchem4040028.
18. Thatyana M, Dube NP, Kemboi D, Manicum ALE, Mokgalaka-Fleischmann NS, Tembu J V. Advances in Phytonanotechnology: A Plant-Mediated Green Synthesis of Metal Nanoparticles Using Phyllanthus Plant Extracts and Their Antimicrobial and Anticancer Applications. Nanomaterials 2023;13. https://doi.org/10.3390/nano13192616.
19. Devi GK, Suruthi P, Veerakumar R, Vinoth S, Subbaiya R, Chozhavendhan S. A review on metallic gold and silver nanoparticles. Res J Pharm Technol 2019;12:935–43. https://doi.org/10.5958/0974-360X.2019.00158.6.
20. Billah AAM, Babu RH, Kiran KD, Bubalan K, Bhuvaneshwari G, Munuswamy K, Reddy KTK, Krishnan K. Phyto-Nanotechnology for Cancer Therapy: A Review of Plant-Mediated Organic Nanoparticles for Targeted Drug Delivery. Journal of Chemical Reviews 2025;7:131–65. https://doi.org/10.48309/jcr.2025.501932.1410.
21. Ngungeni Y, A. Aboyewa J, Moabelo KL, Sibuyi NRS, Meyer S, Onani MO, Meyer M, Madiehe AM. Anticancer, Antioxidant, and Catalytic Activities of Green Synthesized Gold Nanoparticles Using Avocado Seed Aqueous Extract. ACS Omega 2023;8:26088–101. https://doi.org/10.1021/acsomega.3c02260.

22. Nisha, Sachan RSK, Singh A, Karnwal A, Shidiki A, Kumar G. Plant-mediated gold nanoparticles in cancer therapy: exploring anti-cancer mechanisms, drug delivery applications, and future prospects. Frontiers in Nanotechnology 2024;6. https://doi.org/10.3389/fnano.2024.1490980.
23. Hano C, Abbasi BH. Plant-based green synthesis of nanoparticles: Production, characterization and applications. Biomolecules 2022;12. https://doi.org/10.3390/biom12010031.
24. Fahim M, Shahzaib A, Nishat N, Jahan A, Bhat TA, Inam A. Green synthesis of silver nanoparticles: A comprehensive review of methods, influencing factors, and applications. JCIS Open 2024;16. https://doi.org/10.1016/j.jciso.2024.100125.
25. Rauf S, Hameed H, Tariq M, Afareen A, Gulfaraz S, AlKubaisi NA, Elshikh MS. Phytochemical-Mediated Synthesis and Characterization of Silver Nanoparticles Using Mirabilis jalapa Leaf Extract and Their Antibacterial. Microsc Res Tech 2025;88:1795–805. https://doi.org/10.1002/jemt.24801.
26. Sajini T, Joseph J. Microwave-assisted synthesis of nanomaterials: a green chemistry perspective and sustainability assessment. RSC Sustainability 2025. https://doi.org/10.1039/D5SU00584A.
27. Khan F, Shariq M, Asif M, Siddiqui MA, Malan P, Ahmad F. Green Nanotechnology: Plant-Mediated Nanoparticle Synthesis and Application. Nanomaterials 2022;12. https://doi.org/10.3390/nano12040673.
28. Anju Kumari, Vartika Jain. Phytochemical composition and GC-MS analysis of Hymenodictyon orixense Mabb. leaves. GSC Biological and Pharmaceutical Sciences 2025;32:156–79. https://doi.org/10.30574/gscbps.2025.32.3.0357.
29. Reddy M, Chaturvedi A. Pharmacognostical studies of Hymenodictyon orixence (Roxb.) Mabb. leaf. Int J Ayurveda Res 2010;1:103. https://doi.org/10.4103/0974-7788.64400.
30. Chakraborty P, Sasi S, Nair AA, Anjum N, Tripathi YC. Organic & Medicinal Chem IJ Medicinal Applications, Phytochemistry and Pharmacology of Hymenodictyon excelsum (Roxb.) Wall: A Review. Roxb) Wall: A Review Organic & Medicinal Chemistry International Journal 2017;2:1–5. https://doi.org/10.19080/OMCIJ.2017.02.555589.
31. Charan Sahoo P, Bandhu Das Ψ A. Cytotoxic potential of bark extract of Hymenodictyon orixense (Roxb.) Mabb.-a medicinally important tree, on root meristematic tissues of Allium cepa L. Plant Science Research. Plant Science Research 2017;39:59–63.

32. Khairunnisa K, Karthik D. Evaluation of in-vitro apoptosis induction, cytotoxic activity of hymenodictyon excelsum (roxb) wall in dalton's lymphoma ascites (DLA) and lung fibroblast - mouse l929 cell lines. J Appl Pharm Sci 2014;4:11–7. https://doi.org/10.7324/JAPS.2014.40803.
33. Akter R, Uddin SJ, Grice ID, Tiralongo E. Cytotoxic activity screening of Bangladeshi medicinal plant extracts. J Nat Med 2014;68:246–52. https://doi.org/10.1007/s11418-013-0789-5.
34. Chakraborty M, Karmakar I, Haldar PK, Nepal A, Bala a. Cytotoxic and anti proliferative activity of Hymenodictyon excelsum IN Ehrlich ascites carcinoma bearing mice: in vitro and in vivo studies. n.d.
35. Mijanur Rahman M. Pharm Prod. vol. 10. 2015.
36. Evaluation of in vitro and in vivo antimalarial activity of Hymenodictyon excelsum bark extract n.d.
37. Sultana N, Islam MT, Vinícius M, Barros De Alencar O, Wanessa S, Silva C, Chowdhury MU, Amelia A, Melo-Cavalcante C, Mendes De Freitas R. African Journal of Pharmacy and Pharmacology Phyto-pharmacological screenings of two Rubiaceae family plants 2015;9:775–82. https://doi.org/10.5897/AJPP2015.
38. Tripathi YC, Tewari D, Upadhyay L, Tripathi YC, Chakraborty P. Phytochemical Evaluation and Antiinflammatory Effects of Hymenodictyon excelsum (Roxb.) Wall Grown in Uttarakhand State of India. Article in Journal of Pharmacy Research 2016;10:199–204. https://doi.org/10.6084/m9.figshare.3201256.v1.
39. Govindarajan M, Benelli G. One-pot green synthesis of silver nanocrystals using Hymenodictyon orixense: A cheap and effective tool against malaria, chikungunya and Japanese encephalitis mosquito vectors? RSC Adv 2016;6:59021–9. https://doi.org/10.1039/c6ra10228j.
40. Suchaichit N, Kanokmedhakul S, Kanokmedhakul K, Moosophon P, Boonyarat C, Plekratoke K, Tearavarich R, Suchaichit NP. Phytochemical investigation and acetylcholinesterase inhibitory activity of bark of Hymenodictyon orixense. Nat Prod Res 2018;32:2936–9. https://doi.org/10.1080/14786419.2017.1389930.
41. Soun-Udom M, Choowongkomon K, Vajrodaya S, Ratanabunyong S, Suksungworn R, Srisombat N, Bapia S, Duangsrisai S. Antioxidant and anti-HIV properties and isolation of bioactive compound of Hymenodictyon orixense (Roxb.) Mabb. Agriculture and Natural Resources 2019;53:621–8. https://doi.org/10.34044/j.anres.2019.53.6.09.

42. Prasanth Vs, Gopinath C, Aruna K, Lahari S. Antioxidant & Anti Bacterial Activities Of Sliver Nano Particles Biosynthesized From Aqueous Leaf Extract Of Hymenodictyon Orixense M pharmacy student Department of pharmaceutical chemistry JNTUA-OTPRI, Jawaharlal nehru technological university. n.d.
43. Das PP, Das A, Das AB. Phytochemical Credentials, Antimicrobial Activities And Cytotoxicity Of Bark Derived Coumarin of A Medicinally Important Tree Hymenodicton Orixense (ROXB.) MABB. Article in World Journal of Pharmacy and Pharmaceutical Sciences 2022. https://doi.org/10.20959/wjpps202211-23556.
44. Tanamatayarat P, Limtrakul P-N, Chunsakaow S, Duangrat C, ชรวรรณ พ, นอมาตยรั ตน ต, ลิ ้ มตระกู ล พ, นี ส, จั ย, สกาว น, ชฎารั แ, ดวงรั ตน ต. Screening of Some Rubiaceous Plants for Cytotoxic Activity Against Cervix Carcinoma (KB-3-1) Cell Line การคั ดกรองความเป นพิ ษต อเซลล มะเร็ งปากมดลู ก ชนิ ด KB-3-1 ของพื ช บางชนิ ดในวงศ RUBIACEAE. n.d.
45. Hkeem Ibrahem K. Green Synthesis of Nanoparticles Using Plants: (Article Review) 2025. https://doi.org/10.58928/ku24.16210.
46. Karkamkar K, Raj F, Langote S, Shah H, Shivsharan RR, Patil V. Phytochemical-Mediated Synthesis of Silver Nanoparticles from Piper betle and Psidium guajava: A Sustainable Approach to Oral Care Creative Commons 2025;2:122–9. https://doi.org/10.5281/zenodo.16199991.
47. Shaikh JR, Patil M. Qualitative tests for preliminary phytochemical screening: An overview. Int J Chem Stud 2020;8:603–8. https://doi.org/10.22271/chemi.2020.v8.i2i.8834.
48. Mohan C, Devi S. LC-MS and HPTLC Profile of Crude Ethanol Extract of Plant Michelia champaca Linn. Pharmacognosy Res 2024;16:490–4. https://doi.org/10.5530/pres.16.3.59.
49. Vasava P, Chakraborthy GS. Chromatographic Analysis of Polyherbal Extract and Formulation by HPTLC and GC-MS Methods. Journal of Natural Remedies 2025;25:113–9. https://doi.org/10.18311/jnr/2025/43942.
50. Moulishankar A. Significance of TLC and HPTLC in Phytochemical Screening of Herbal Drugs. 2021.
51. Firmansyah A, Winingsih W, Manobi JDY. Review of scopoletin: Isolation, analysis process, and pharmacological activity. Biointerface Res Appl Chem 2021;11:12006–19. https://doi.org/10.33263/BRIAC114.1200612019.
52. Prashad Sharma B, Patra A, Kumar Sahu B, Jena N, Lal S. Phytochemical screening and TLC profiling of Argemone mexicana L. (Svarnakshiri) flowers Phytochemical screening

and TLC profiling of Argemone mexicana L. (Svarnakshiri) flowers Licensed under a Creative Commons Attribution 4.0 International License. Medico-Biowealth of India 2025;19. https://doi.org/10.5281/zenodo.14880856.

53. Dinesh R, India RR. LCMS-A Review And A Recent Update. Dinesh et al World Journal of Pharmacy and Pharmaceutical Sciences 2016;5:377. https://doi.org/10.20959/wjpps20165-6656.
54. Javed R, Ijaz S, Hameed H, Nazish M, Sharif MS, Afreen A, Alarjani KM, Elshikh MS, Mehboob S, Abdul Razak S, Waheed A, Ahmed R, Tariq M. Phytochemical-Mediated Biosynthesis of Silver Nanoparticles from Strobilanthes glutinosus: Exploring Biological Applications. Micromachines (Basel) 2023;14. https://doi.org/10.3390/mi14071372.
55. Abeysinghe DT, Kumara KAH, Kaushalya KAD, Chandrika UG, Alwis DDDH. Phytochemical screening, total polyphenol, flavonoid content, in vitro antioxidant and antibacterial activities of Sri Lankan varieties of Murraya koenigii and Micromelum minutum leaves. Heliyon 2021;7. https://doi.org/10.1016/j.heliyon.2021.e07449.
56. Chandran KC, Kavitha Chandran CC. Quantitative estimation of total phenolic, flavonoids, tannin and chlorophyll content of leaves of Strobilanthes Kunthiana (Neelakurinji). vol. 4. 2016.
57. Nandihalli N. Microwave-driven synthesis and modification of nanocarbons and hybrids in liquid and solid phases. J Energy Storage 2025;111. https://doi.org/10.1016/j.est.2025.115315.
58. Grewal AS, Singh Grewal A, Kumar K, Redhu S, Bhardwaj S, Nayak J, Devi C. Microwave assisted synthesis: a green chemistry approach Sonika Redhu Microwave Assisted Synthesis: A Green Chemistry Approach. International Research Journal of Pharmaceutical and Applied Sciences 2013;3:278–85.
59. Li Z, Peng K, Ji N, Zhang W, Tian W, Gao Z. Advanced mechanisms and applications of microwave-assisted synthesis of carbon-based materials: a brief review. Nanoscale Adv 2024;7:419–32. https://doi.org/10.1039/d4na00701h.
60. Dwivedi A, Das S, Tiwari V, Yadav V, Jain SK, Mandal V, Mukherjee S, Satpathy S, Mohapatra D, Sahu AN, Satpathy MP, Mehta SK, Singh S, Goyal M, Kazi M, Hussain MD, Patra A. Microwave-assisted green synthesis of silver nanoparticles using Mitragyna parvifolia bark extract and their biological activities: an economical and environment-friendly approach. Green Chem Lett Rev 2024;17. https://doi.org/10.1080/17518253.2024.2395919.

61. Rama P, Mariselvi P, Sundaram R, Muthu K. Eco-friendly green synthesis of silver nanoparticles from Aegle marmelos leaf extract and their antimicrobial, antioxidant, anticancer and photocatalytic degradation activity. Heliyon 2023;9. https://doi.org/10.1016/j.heliyon.2023.e16277.
62. Akinwumi Gentle A, Qudus Omogbolahan S, Oluwatosin Godwin J. Characterization Of Biosynthesized Silver Nanoparticles Using UV-Visible And FTIR Spectroscopy. African Journal of Environment and Natural Science Research 2020;3:21–6.
63. Ramzan M, Abusalah M, Ahmed N, Yean C, Zeshan B. Green Synthesis and Characterization of Silver Nanoparticles Using Zingiber officinale Extracts to Investigate Their Antibacterial Potential. Int J Nanomedicine 2024;Volume 19:13319–38. https://doi.org/10.2147/IJN.S475656.
64. Chaudhary S, Jyoti A, Singh Tomar R, Shrivastava V. Phytochemical mediated synthesis and characterization of Iron Nanoparticles using Saraca asoca leaves extract. International Journal of Pharmaceutical and Phytopharmacological Research 2020;10:1–147. https://doi.org/10.13140/RG.2.2.24149.45287.
65. Saraswat A, Kumar A. Microwave-assisted synthesized Co-doped Fe3O4 nanoparticles for superior electrocatalytic water splitting. Discover Nano 2025;20. https://doi.org/10.1186/s11671-025-04285-9.
66. Agarwal H, Venkat Kumar S, Rajeshkumar S. Antidiabetic effect of silver nanoparticles synthesized using lemongrass (Cymbopogon citratus) through conventional heating and microwave irradiation approach. Journal of Microbiology, Biotechnology and Food Sciences 2018;7:371–6. https://doi.org/10.15414/jmbfs.2018.7.4.371-376.
67. Mukherjee S, Chandrakar M, Gupta P, Khan A, Pal R, Dwivedi A, Chouhan KBS, Das S, Patra A, Mandal V. A two-stage extraction model for simultaneous extraction of essential oil and phenolics from tulsi leaves: implementing a blended mode microwave hydrodiffusion and gravity (MHG) model. Sustainable Food Technology 2024. https://doi.org/10.1039/d4fb00177j.
68. Naseem K, Ur Rehman MZ, Ahmad A, Algarni TS, Dubal D. Plant extract induced biogenic preparation of silver nanoparticles and their potential as catalyst for degradation of toxic dyes. Coatings 2020;10:1–15. https://doi.org/10.3390/coatings10121235.
69. Miah MY, Halder S, Saikat SP, Dewanjee S, Ashaduzzaman M, Bhowmik S. Microwave-assisted one-step synthesis of polyacrylamide/NiO nanocomposite for biomedical applications. RSC Adv 2025;15:18971–85. https://doi.org/10.1039/d5ra02496j.

70. Alharbi NS, Alsubhi NS. Green synthesis and anticancer activity of silver nanoparticles prepared using fruit extract of Azadirachta indica. J Radiat Res Appl Sci 2022;15:335–45. https://doi.org/10.1016/j.jrras.2022.08.009.
71. Raletsena M V., Mongalo NI. Phytochemical analysis, in vitro antimicrobial, anticancer, anti-inflammatory, and antioxidant activity of extracts from Bulbine anguistifolia Poelln (Asphodelaceae). South African Journal of Botany 2023;159:588–95. https://doi.org/10.1016/j.sajb.2023.06.044.
72. Venugopal K, Rather HA, Rajagopal K, Shanthi MP, Sheriff K, Illiyas M, Rather RA, Manikandan E, Uvarajan S, Bhaskar M, Maaza M. Synthesis of silver nanoparticles (Ag NPs) for anticancer activities (MCF 7 breast and A549 lung cell lines) of the crude extract of Syzygium aromaticum. J Photochem Photobiol B 2017;167:282–9. https://doi.org/10.1016/j.jphotobiol.2016.12.013.
73. Joshi P, Pandey L kant, Misra V, Patel A, Singh R, Baksh Z. Green Synthesis and Characterization of Silver Nanoparticles Using Stachytarpheta indica. Int J Curr Microbiol Appl Sci 2025;14:16–24. https://doi.org/10.20546/ijcmas.2025.1404.004.
74. Al-Malki WF, Alharbi NS. Ficus Plant-Mediated Silver Nanoparticles: Synthesis, Optimization, Characterization, and Biomedical Applications. J Pure Appl Microbiol 2025;19:74–99. https://doi.org/10.22207/JPAM.19.1.58.
75. Edo GI, Mafe AN, Ali ABM, Akpoghelie PO, Yousif E, Isoje EF, Igbuku UA, Zainulabdeen K, Owheruo JO, Essaghah AEA, Umar H, Ahmed DS, Alamiery AA. Eco-friendly nanoparticle phytosynthesis via plant extracts: Mechanistic insights, recent advances, and multifaceted uses. Nano TransMed 2025;4. https://doi.org/10.1016/j.ntm.2025.100080.